

DIELECTRIC LOSS ESTIMATION

USING

DAMPED AC VOLTAGES

S.A.A. Houtepen

High Voltage Technology and Management
Department of Electrical Sustainable Energy
Faculty of Electrical Engineering, Mathematics and Computer Science
Delft University of Technology, June 2010

DIELECTRIC LOSS ESTIMATION USING DAMPED AC VOLTAGES

S.A.A. Houtepen

June 1, 2010

Thesis Committee

prof. dr. J.J. Smit

dr.-hab.ir. E. Gulski

dr.ir. M. Popov

PREFACE

For the completion of my MSc study in Electrical Power Engineering, I performed a research project at the department of High Voltage Technology and Management of the Delft University of Technology. This investigation focused on the dielectric loss measurement with damped AC Voltages. In this report, a presentation of this research is given.

For a more detailed description of the physics behind dielectric losses and aging of insulation, one is referred to chapter 2. In chapter 3, a mathematical representation is given on a damped AC system, which is compared to a more detailed model. For a thorough investigation on ways to determine the attenuation from a DAC wave as stable as possible, details can be found in chapter 4. The determination of the internal system losses are described in chapter 5, and a complete overview of dielectric loss estimation using damped AC is given in chapter 6. This report is finalized with conclusions and recommendations in chapter 7.

I would like to thank my supervisors during this project; dr.-hab. ir. Edward Gulski from the Delft University of Technology, and dr. ir. Ben Quak from Seitz Instruments AG in Switzerland. Without the help and discussions, I was not able to do this research and write this report. Secondly, I also want to thank Piotr Cichecki, for providing me with a large amount of measurement data from the field. Last, but not least, I would like to thank my parents, John and Marianne, for giving me the opportunity to do this and for the support they gave me during the years I went to college.

Delft, May 2010

Richard Houtepen

SUMMARY

Dielectric loss measurement is one of most important diagnostic tools for condition assessment of e.g. oil-filled cables. One of the methods to determine the loss tangent is based on damped AC voltages.

Since 10 years, the use of damped AC (DAC) voltages is a well known method to determine $\tan \delta$. In particular the estimation of dielectric loss parameter is based on the estimation of the DAC voltage attenuation, and numeric procedures are used. To achieve sufficient sensitivity (at this moment 0.1%), each type of system has to be subjected to a detailed calibration procedure. Due to the fact, that damped AC voltage becomes more and more a standard solution for on-site diagnosis of all types of oil-filled power cables up to 380kV and stator insulation of electrical machines, systematic research is necessary to optimize the procedure of dielectric loss estimation.

This study consists mainly of three parts. These are:

- Derivation and determination of a proper model for further calculations
- Investigation on methods to determine the total losses from the DAC wave
- Research on the calibration of a DAC system, to eliminate internal system losses

The second and third parts are based on empirical research, and therefore give a fundamental basis for final conclusions.

The mathematical model showed that a representation of a DAC system with one total equivalent internal resistance is most suitable for use. This is due to the fact that a more detailed model (with every component separately modelled) results in a negligible improvement and secondly creates an unmanageable situation (all components are voltage/frequency dependent and component calibration should be applied).

To investigate the total losses from a DAC system, two arbitrary peaks of the wave have to be taken and via a calculation this will result in the dielectric losses. In theory, it should not matter which two peaks and/or lows are taken. In practice however, it is clear that an offset is present. Therefore, a new and more robust method is presented. This method calculates the attenuation from the first two peaks, and averages it with the attenuation from the first two lows.

When the total losses are determined, the internal system losses have to be obtained via a detailed calibration and subtracted during future measurements. Since these losses are voltage/frequency dependent, an extensive calibration is currently in use. This procedure consists of a parallel and series switching of several test capacitors (in order to create different frequencies). If this is done in a wide range of voltages, a 3D relationship originates between voltage, capacitance and internal resistance. From the obtained internal resistance values, the (known and very low) losses caused by the test capacitors are eliminated.

In this thesis, research is done on a way to simplify this procedure by changing from a capacitance to a frequency scale. This resulted in a more linear depiction of the obtained results for the internal resistance. Linearization of these frequency scaled values is investigated and although the trend line of the dielectric losses in function of voltage remained the same, more inaccuracy of the absolute value of the dielectric losses was the result. It is therefore recommended to use the current calibration procedure, in order to maintain the current high accuracy of the dielectric loss calculation.

In order to calculate the dielectric losses from a damped AC voltage wave, the following steps have to be taken;

- Determine the attenuation of the DAC wave, by averaging the obtained value for the attenuation coefficient from two peaks and two lows.
- If the internal losses are unknown, calibrate the system at different voltages and frequencies.
- If the system losses are known, determine these losses at that particular voltage and frequency.
- Calculate the dielectric losses of the system, with the use of a mathematical model consisting of one total equivalent internal resistance.

TABLE OF CONTENTS

Preface	III
Summary	V
Table of Contents	VII
1. Introduction	1
1.1 Introduction to Condition Assessment.....	1
1.2 On-Site Testing of HV Equipment.....	3
1.3 Problem Definition and Scope of this Study.....	4
2. Dielectric Losses	5
2.1 Physical Background of Dielectric Losses.....	5
2.1.1 Definition.....	5
2.1.2 Origin.....	7
2.1.2.1 Dipole Losses	7
2.1.2.2 Conductive Losses	9
2.1.2.3 Interface Losses	10
2.1.2.4 Discharge Losses	11
2.2 Aging of Insulation.....	12
2.2.1 Oil-Impregnated Insulation.....	12
2.2.1.1 Chemical Structure	12
2.2.1.2 Aging	15
2.2.2 Epoxy-Mica Insulation.....	19
2.2.2.1 Insulation Structure	19
2.2.2.2 Causes of Defects	20
2.2.2.3 Deterioration	21
2.2.2.4 Effects on $\tan \delta$	22
2.3 Measurement Techniques.....	23
2.3.1 Continuous Energizing.....	23
2.3.1.1 Very Low Frequency Analysis	23
2.3.1.2 The Schering Bridge	24
2.3.1.3 Dielectric Spectroscopy	25
2.3.2 Temporarily Energizing.....	26
2.3.2.1 Return Voltage Measurement	26
2.3.2.2 Damped AC	27
3. Damped AC Voltages	31
3.1 Principle of Electrical Resonance.....	31
3.1.1 Modelling a series RLC Circuit.....	32
3.1.1.1 Mathematical Derivation	32
3.1.1.2 Attenuation β and Quality factor Q	34
3.2 A Mathematical Model of a DAC System.....	35
3.2.1 Mathematical Derivation.....	35
3.3 A More Detailed Model.....	39
3.3.1 Mathematical Derivation.....	39

4.	Loss Calculation using DAC	43
4.1	Introduction to Attenuation Coefficient β	43
4.2	The Different Calculation Methods.....	45
4.2.1	Theoretical Approach.....	45
4.2.2	Attenuation in Practice.....	46
4.3	Including an Offset.....	50
4.3.1	Introduction.....	50
4.3.2	Positive Offset.....	50
4.3.2.1	<i>A Small Offset</i>	50
4.3.2.2	<i>An Extreme Value</i>	51
4.3.3	Negative Offset.....	52
4.3.3.1	<i>A Small Offset</i>	52
4.3.3.2	<i>An Extreme Value</i>	52
4.3.4	Observations.....	53
4.4	A New Calculation Method for β	54
4.4.1	Introduction.....	54
4.4.2	Application to Measurement Data.....	54
4.4.2.1	<i>Effects of an Offset</i>	54
4.4.2.2	<i>Influence on the Voltage Trendline</i>	59
4.5	Chapter Conclusions.....	62
5.	The Internal System Losses	63
5.1	The Current Calibration Procedure.....	63
5.2	Investigation on the Calibration Matrices.....	65
5.2.1	An Experimental Approach.....	65
5.2.2	Practical Support.....	66
5.2.2.1	<i>A 28 kV DAC System</i>	66
5.2.2.2	<i>A 60 kV DAC System</i>	69
5.2.2.3	<i>A 150 kV DAC System</i>	70
5.2.3	Observations.....	70
5.3	Linearization of the Frequency Representation.....	71
5.3.1	The Applied Method.....	71
5.3.2	Validation of the Linear Method.....	72
5.3.3	Remarks.....	76
5.4	Chapter Conclusions.....	77
6.	A Complete Overview	79
6.1	Flow Chart.....	79
6.2	Procedure Explanation.....	80
7.	Conclusions and Recommendations	83
	References	IX
	Appendix A: Matlab Code MSc Thesis	XIII
	Appendix B: CMD 2010 Conference Proceeding	XIX

1 ● INTRODUCTION

1.1 Introduction to Condition Assessment

In the current society, the dependency on electrical energy is enormous and an interruption of the power supply becomes more and more an unaccepted occurrence. The liberalization of the energy market resulted in utility companies that are forced to obtain a competitive edge. Therefore, more focus was put on maintenance and condition assessment of HV equipment and a policy in which the installed components should be fully used up till the end of their lifetime originates.

Combined with the continuously increasing demand for flexibility and reliability of electrical energy supply, grid utility companies face enormous challenges in maintaining an appropriate balance between the reliability of the energy distribution on one hand and a grid whose components suffer from aging due to electrical and thermal stresses on the other hand.

In the Netherlands, for example, XLPE cables are commonly installed at the moment in high voltage networks [4]. Before the 1980's however, large numbers of oil impregnated cables were taken into operation, and much of those components are still in service today. Failures in the Dutch transmission system are nevertheless rare, and the knowledge about the actual condition and aging processes in these systems is still limited. The same can be said on the actual condition of stator bar insulation in electrical machines, which have a leading role in the generation of electrical energy.

Condition Assessment

Nowadays, many advanced methods for condition assessment of service-aged HV components are available. These condition assessment diagnostics, which are applied to service-aged HV systems, are not only based on a pass or fail criterion. During such a test, attention is paid to recognize, localize and evaluate possible defects. When this is done periodically, evaluation of these processes in time can be monitored.

The main purposes of condition assessment of HV equipment are listed hereunder [4]:

- To check the availability and reliability of the component
- By non-destructive diagnostics, it can be estimated what the actual condition of the service-aged system is, and a check is performed on the insulation degradation after a period in time.
- Reference values of the diagnostic tools are provided and can be used for later tests (in order to demonstrate whether the insulation is still free from dangerous defects and that the life-time expectation is sufficiently high)
- Diagnostic measurements can demonstrate that a component has been successfully repaired after a failure and the defect in the insulation is eliminated

To assess the dielectric properties of high-voltage equipment in service, non-destructive methods are used. One of the major techniques to determine the dielectric properties of electrical insulation in a non-destructive way is via the dielectric loss parameter $\tan \delta$.

In the next paragraphs, a detailed description of the physical background and major measurement techniques of this loss tangent are presented.

1.2 On-Site Testing of HV Equipment

Energizing and testing components with a high capacitance (e.g. long cables) at an AC overvoltage demands reactive power of several MVA, which can impossibly be supplied by mobile installations.

An example with specifications from one of the largest conventional mobile installations available is given below. It can be seen here; that the limitation of this particular test transformer includes a maximum capacitance of 1.6 uF which can be tested at 260 kV.

Unit	Maximum value
Voltage	260 kV
Inductance	16.2 H
Current	83 A
Load capacitance at max. voltage	18-1600 nF
Frequency range	20-300 Hz
Lowest frequency at max. voltage	31 Hz

Table 1-1: Example of specifications from a test transformer for on-site testing

When concerning e.g. long power cables, the capacitance of the test object can go up to 10 uF. To reduce the reactive power required, it is therefore common to test at VLF (0.1 Hz) or DC voltage. With the advent of damped AC, a new method is applicable that can go up to 350 kV and multiple micro-farad's. Furthermore, the test equipment can be transported in a minivan which makes is very suitable for on-site testing.

In this research, the main focus is on the dielectric loss estimation using these damped AC voltages.

1.3 Problem Definition and Scope of this Study

Problem Definition

Dielectric loss measurement is one of most important diagnostic tools for condition assessment of e.g. oil-filled cables. One of the methods to determine the loss tangent is based on damped AC voltages.

Since 10 years, the use of damped AC (DAC) voltages is a well known method to determine $\tan \delta$. In particular the estimation of dielectric loss parameter is based on the estimation of the DAC voltage attenuation, and numeric procedures are used. To achieve sufficient sensitivity (at this moment 0.1%), each type of system has to be subjected to a detailed calibration procedure. Due to the fact, that damped AC voltage becomes more and more a standard solution for on-site diagnosis of all types of oil-filled power cables up to 380kV and stator insulation of electrical machines, systematic research is necessary to optimize the procedure of dielectric loss estimation.

Scope of this Study

The goals of this MSc. Thesis are:

1. Inventarisation of knowledge on dielectric losses
 - a. Give an overview on the physical processes and measurement techniques
2. Derivation of a mathematical model of a damped AC system, which can be used for further investigation on DAC voltages.
3. Theoretical investigation on methods to determine signal losses from attenuated waves, and give a proposal of improvement for this calculation.
 - a. Present an overview of possible methods.
 - b. Comparison between the investigated methods and the method that is currently used in the DAC system (e.g. OWTS technology).
 - c. Determine whether the total accuracy and overall stability of this calculation can be increased further (e.g. another calculation method).
 - d. Propose an improvement in the calculation of losses from damped oscillations, which is suitable for implementation in a DAC -system.
4. Investigation on the determination of internal system losses, and propose improvements for the current calibration procedure.
 - a. Research on the current calibration procedure and resulting calibration matrices.
 - b. Give possible improvements that reduce the current extensive calibration procedure without the loss of accuracy.

2. DIELECTRIC LOSSES

2.1 Physical Background of Dielectric Losses

2.1.1 Definition

When a voltage is applied, a potential difference to earth is created and an electric field originates in the insulation material (dielectric). In a cable for example, the electric field can be calculated using [2-1].

$$E = \frac{V}{r \ln\left(\frac{b}{a}\right)} \quad [kV / mm] \quad [2-1]$$

Where V is in kV, r in mm, and a and b are the distances from the center to respectively the inner and outer boundary of the insulation material. E then becomes the electric field in kV/mm.

Due to the present potential difference, a capacitive current starts to flow in the dielectric. This current leads the voltage across the dielectric by 90 degrees.

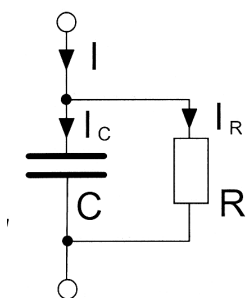


Figure 2-1:
Parallel Equivalent Circuit; only valid for one voltage level / frequency at a time

In practice however, there is no such thing as a perfect insulator, and a small amount of losses is unavoidable. The dielectric can therefore be represented by the equivalent circuit in figure 2-1, with C as the lossless component and R as the lossy component of the insulation [1].

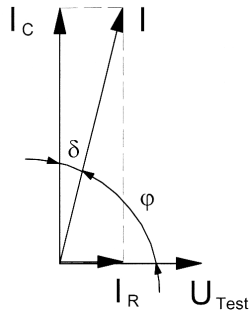


Figure 2-2:
Dielectric Loss angle δ and Power Factor angle φ

Due to these dielectric losses, the net current vector is shifted by an angle δ . A graphic plot is given in figure 2-2. An important measure for the dielectric losses is thus the so-called loss-factor $\tan \delta$. When using the parallel circuit of figure 1-1, the loss factor can be calculated with [2-2].

$$\tan(\delta) = \frac{I_R}{I_C} = \frac{U/R}{U\omega C} = \frac{1}{\omega RC} \quad [2-2]$$

The absolute value of the dielectric losses (in Watts) is related to this angle δ and varies with the square of the voltage according to [2-3]. It is thus a measure for the energy dissipation through and over the surface of the insulation.

$$W = U \cdot I_C \cdot \tan(\delta) = U^2 \cdot \omega \cdot C \cdot \tan(\delta) \quad [Watts] \quad [2-3]$$

The dissipation factor can also be determined by dividing the real power over the reactive power [2-4], or as a function of φ , the power factor angle.

$$\tan(\delta) = \frac{P}{Q} = \frac{UI \cos(\varphi)}{UI \sin(\varphi)} = \frac{\cos(\varphi)}{\sin(\varphi)} \quad [2-4]$$

The cosine of φ represents the power factor. Some typical values of the loss tangent for different materials are shown in figure 2-3.

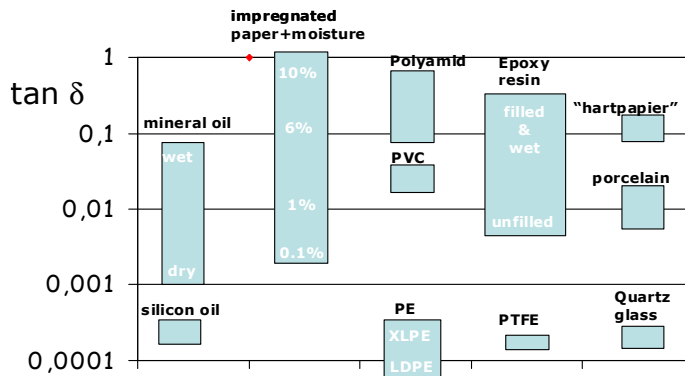


Figure 2-3:
Typical values for the loss tangent of different materials [9]

2.1.2 Origin

The resistive component in figure 2-1 can represent four kinds of losses, which are described in detail in the following sections [1];

- Dipole losses
- Conduction losses
- Interface losses
- Partial discharges

2.1.2.1 Dipole losses

Every particle (e.g. atoms, molecules) in a material consists of positive and negative charges. Under the influence of an electric field, these charges are slightly displaced from each other (orientated), and are referred to as dipoles. The origination of dipoles results in a so-called polarization of the dielectric.

Electric dipoles in an insulation material thus constantly reverse direction in an AC-field. Because the dipoles do not lag the field vector at low frequencies, dipole losses mainly occur at higher frequencies (from approximately 30 Hz upwards). When the frequency increases, friction causes the dipoles to lag the field vector and give rise to losses. When the frequency is increased even further, the dipoles can no longer follow, causing the losses to decrease again.

Due to the fact that dipoles respond with a certain delay on changes in the electric field, they lag the field vector by a certain angle. Therefore, the permittivity (dielectric constant) of the material can be written as a complex number, consisting of a magnitude and phase angle. The real part of the permittivity then represents the stored energy in the material, and the complex part represents the dissipation of energy [2-5].

$$\epsilon_r = \epsilon'_r - j\epsilon''_r \quad [2-5]$$

In figure 2-4, the value of the imaginary and real part of the permittivity in a wide frequency range is shown, whereby different polarization processes are visible.

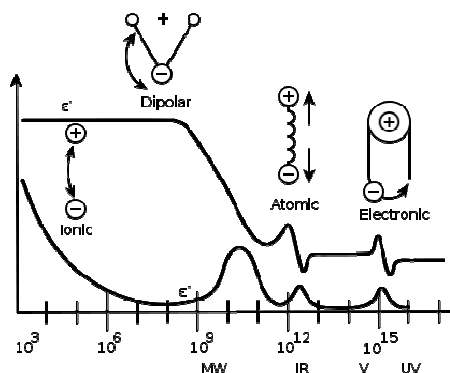


Figure 2-4:
Permittivity as a function of frequency [2]

The polarization processes are briefly described hereunder [3]:

Electronic Polarization

An atom consists of a nucleus with surrounding electrons. If an electric field is applied, the electron density is displaced with respect to the nucleus, and a dipole is born. This effect is extremely fast and can follow the electric field up to very high frequencies.

Atomic Polarization

When the applied field causes an electron cloud to deform, positive and negative charges originate. As with electronic polarization, this dipole can follow up to high frequencies.

Dipolar Polarization

This type of polarization results from permanent dipoles. These dipoles do not get polarized further (the distance between the charges remains constant), but only rotate when influenced by an electric field. Dipolar polarization is still a quite fast effect, which can follow up to MHz to GHz.

Ionic Polarization

The process of ionic polarization occurs when positive and negative ions are displaced from each other. This effect is rather slow, and will not follow up to high frequencies.

Interfacial Polarization

Another effect that is not shown in figure 2-4, is the so-called interfacial polarization. This is the dominant process in insulating materials composed of multiple dielectric materials (e.g. oil impregnated paper). Due to the mismatch in permittivity times resistivity of both materials, positive and negative charges are deposited on the interfaces when an electric field is applied and also form some kind of dipoles. This process is extremely slow, and is only active in the power frequency range and below.

The resistance (figure 2-1) that represents the dipole losses equals [2-6], and the loss tangent then becomes [2-7].

$$R_{pol} = \frac{\epsilon'_r}{\omega C \epsilon''_r} \quad [2-6]$$

$$\tan \delta_{pol} = \frac{1}{\omega R_{pol} C} = \frac{\epsilon''_r}{\epsilon'_r} \quad [2-7]$$

As can be expected, temperature is an important variable in this type of losses, because with increasing temperature dipoles gain a higher mobility. With changing temperature, the earlier discussed frequency spectrum will therefore change.

2.1.2.2 Conductive losses

When the resistance of the dielectric is sufficiently low, the leakage current adds to the dielectric losses. This increased conduction, caused by movement of free charge carriers, can be represented by a conductivity σ . The resistance representation (figure 1-1) then becomes [1-8], and the loss tangent is given by [1-9].

$$R_{\text{Conductivity}} = \frac{\epsilon_0 \cdot \epsilon_r'}{\sigma \cdot C} \quad [1-8]$$

$$\tan \delta_{\text{cond}} = \frac{\sigma}{\omega \epsilon_0 \epsilon_r'} = \frac{1}{\omega \cdot R_{\text{conductivity}} \cdot C} \quad [1-9]$$

Since conduction is caused by a free movement of charge carriers, it is influenced by the applied test voltage (and resulting electric field magnitude) and temperature (a higher charge carrier mobility is gained at elevated temperatures). For this reason, it can further be said that this type of losses mainly occurs at lower frequencies.

The total dielectric losses of an insulation material (healthy and with no interfaces) are determined by the sum of the losses caused by conduction, and those caused by polarization [1-10], [1-11].

$$\tan(\delta) = \tan \delta_{\text{cond}} + \tan \delta_{\text{pol}} \quad [1-10]$$

$$\tan(\delta) = \frac{\sigma}{\omega \epsilon_0 \epsilon_r'} + \frac{\epsilon_r''}{\epsilon_r'} = \frac{1}{\omega \cdot R_{\text{pol}} \cdot C} + \frac{1}{\omega \cdot R_{\text{cond}} \cdot C} = \frac{1}{\omega RC} \quad [1-11]$$

With,

$$R = \frac{R_{\text{pol}} \cdot R_{\text{cond}}}{R_{\text{pol}} + R_{\text{cond}}} \quad [1-12]$$

Figure 2-5 shows the dielectric losses from conduction and polarization in one graph in a wide range of frequencies, combined with the effects of aging on these loss-related processes.

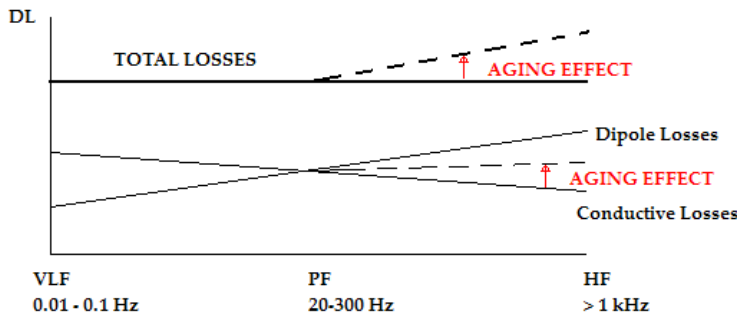


Figure 2-5:
Different loss-related processes in function of frequency with corresponding aging effects

At frequencies below 30 Hz, the conduction losses are the dominant process, whereas above this frequency the dipole losses are the dominant loss mechanism.

2.1.2.3 Interface losses

In many installations, a perfect insulator is used together with a lossy dielectric (e.g. a solid spacer and a gas in a GIS system). The interface between these two materials can be represented by figure 2-6. The loss tangent then becomes [2-13].

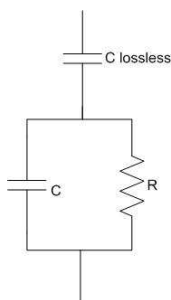


Figure 2-6:
Equivalent circuit of an interface between a lossless and a lossy dielectric

$$\tan \delta = \frac{\omega R K}{1 + \omega^2 R^2 C (K + C)} \quad [2-13]$$

These losses are zero when $\omega=0$ and when $\omega=\infty$, but reach a maximum in-between that is less sharp than with polarization losses. In this way, they can be easily recognized [1].

2.1.2.4 Discharge Losses

Besides polarization and conduction, also partial discharges cause an increase in the loss tangent. In general, three types of PD (discharges that do not completely bridge the distance between the electrodes) can be distinguished [1];

- Internal discharges
- Surface discharges
- Corona discharges

These partial discharges all start at a certain inception voltage (PDIV). At this voltage level, a sudden increase of $\Delta \tan \delta$ occurs (see figure 2-7). Above this inception voltage the dielectric losses start to grow rapidly. PD normally occurs when the voltage is pushed far beyond the nominal value, or if the cable is in bad condition.

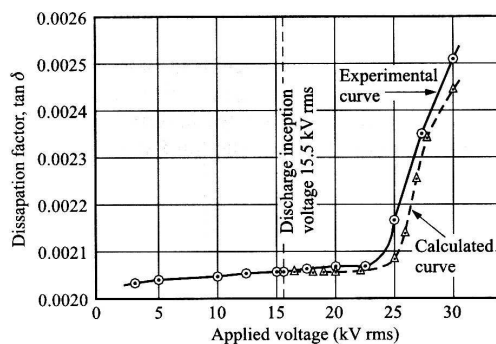


Figure 2-7: Increase in loss tangent above inception voltage PD [9]

The number and magnitude of these discharges also has its effect on the dielectric losses, since it results in a steeper rise of the loss tangent. To identify this type of losses, not the frequency but the voltage should be varied. A result as given in figure 2-7 will appear.

2.2 Aging of Insulation

Due to electrical, mechanical, thermal and environmental stresses, a dielectric ages in time. During this process of aging, irreversible chemical changes occur within the materials that have their influence on the dielectric properties (e.g. dielectric losses) and dielectric strength. Because the dielectric loss parameter an important tool to determine aging in oil impregnated insulation and epoxy-mica, both are described in detail hereunder.

2.2.1 Oil-Impregnated Insulation

For many years, oil impregnated insulation was among the most widely used insulation types in for example high-voltage cables. This generation of HV equipment, however, gradually starts to suffer from aging as large numbers of installed components reach the end of their lifetime expectancy. In this section, a detailed description is given on the material properties of oil impregnated insulation.

2.2.1.1 Chemical Structure

On a microscopic scale, paper consists of cellulose molecules that are connected to each other by oxygen atoms, and form so-called polymer chains. The chemical structure of such a cellulose molecule is given in figure 2-8.

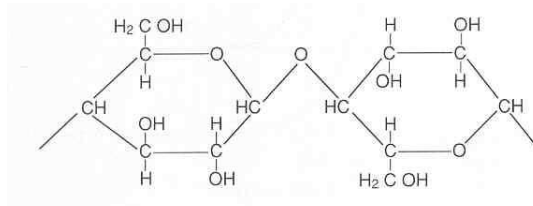


Figure 2-8: Two cellulose molecules, connected by an oxygen atom

To create paper, the moistened cellulose is pressed together, and dried afterwards. This process has to be done with great care, in order to obtain satisfying electrical properties. It goes without saying that when sufficient water molecules remain in the paper, it can be detrimental for the insulation capabilities.

Because of the porous structure of the paper (only 50 to 60 % of the volume consists of cellulose), it is not suitable for practical applications when used alone. Not only pores and free spaces originate in the paper during the production process, also the length of the polymer chains is limited, and free spaces exist in-between (a measure for the length of these chains is the Degree of Polymerization (DP)) [4].

These available pores have the tendency to absorb fair amounts of moisture from the air (up to 8 % of their own weight when stored). To make the paper applicable for practical use, it is therefore impregnated with oil. Oil is chosen for its outstanding electrical, chemical and mechanical properties [5]. Figure 2-9 shows the effects of poorly impregnated cellulose on the dielectric loss tangent. It visualizes the importance of this process.

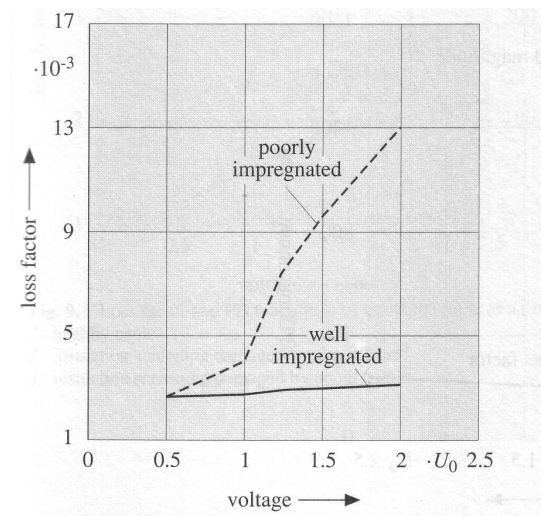


Figure 2-9: Influence of poor impregnation on the dielectric loss tangent [9]

When impregnated properly, the combination of paper impregnated with oil acts as a good insulator. Still, paper is the major variable that determines the dielectric strength, because of its thickness and the way it is layered. This can be explained as follows. The permittivity of paper insulation is around 4.5, while the permittivity of oil is 2.2. Therefore the field strength in the oil is twice the value occurring in paper. In fact, the impulse breakdown strength in oil approaches the intrinsic breakdown value [10]. When the paper layers are thicker, the oil gaps are increased in size, and an avalanche occurs more easily.

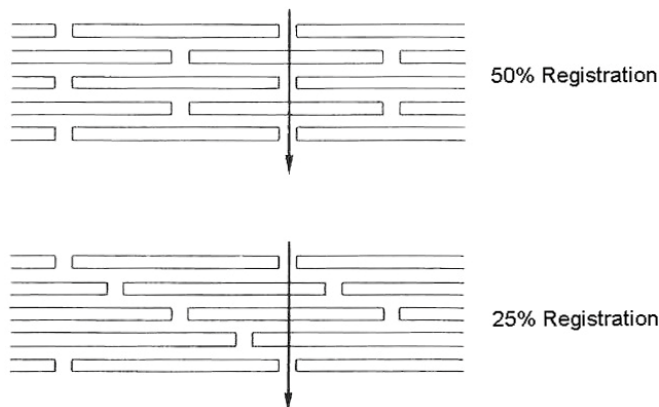


Figure 2-10: Registration values of paper-oil insulation [10]

Secondly, the layering in itself is of importance. Layering is expressed in terms of registration. The percentage registration determines the amount of which a layer is shifted compared to its neighbors (e.g. 25 % registration means it has 75 % overlap with the adjacent layers). Figure 2-10 shows two examples of registration values [10]. The higher the registration, the more gaps are in line, and the lower the breakdown strength. To reduce the stress on the insulation near the conductor at higher voltages, the inner part of the paper layers are made thinner than the ones on the outer part [5].

It can further be said, that the combination of two materials also has its effect on the polarization processes. These processes (of paper and oil) behave differently in each of both materials. In insulation consisting of multiple layers, the dominant polarization process is boundary polarization [6].

Finally, due to the fact that degradation of both materials in oil impregnated insulation does influence each other, aging in most cases can be described by just one parameter, the p-factor [7]. The lower this value is, the better the condition of the dielectric.

2.2.1.2 Aging

Aging of insulation is a very complex process that constantly continues during the entire service life. In table 2-1, an overview is presented on the acting age factors with corresponding aging mechanisms [8].

Ageing Factor	Ageing Mechanisms	Effects*
Thermal		
High temperature Temperature cycling	-Chemical reaction -Incompatibility of materials -Thermal expansion (radial and axial) -Diffusion -Anneal locked -in mechanical stresses -Melting/flow of insulation	-Hardening, softening, loss of mechanical strength, embrittlement -Increase tan delta -Shrinkage, loss of adhesion, separation, delamination at interfaces -Swelling -Loss of liquids, gases -Conductor penetration -Rotation of cable -Formation of soft spots, wrinkles -Increase migration of components
Low temperature	-Cracking -Thermal contraction	-Shrinkage, loss of adhesion, separation, delamination at interfaces -Loss/ingress of liquids, gases -Movement of joints, terminations
Electrical		
Voltage, ac, dc, Impulse	-Partial discharges (PD) -Electrical treeing (ET) -Water treeing (WT) -Dielectric losses and capacitance -Charge injection -Intrinsic breakdown	-Erosion of insulation→ET -PD -Increased losses and ET -Increased temperature, thermal ageing, thermal runaway -Immediate failure
Current	-Overheating	-Increased temperature, thermal ageing, thermal runaway
Mechanical		
Tensile, compressive, shear stresses, Fatigue, cyclic bending, vibration	-Yielding of materials -Cracking -Rupture	-Mechanical rupture -Loss of adhesion, separation, delamination at interfaces -Loss/ingress of liquids, gases
Environmental		
Water/humidity Liquids/gases Contamination	-Dielectric losses and capacitance -Electrical tracking -Water treeing -Corrosion	-Increased temperature, thermal ageing, thermal runaway -Increased losses and ET -Flashover
Radiation	-Increase chemical reaction rate	Hardening, softening, loss of mechanical strength, embrittlement

* The failure mechanism is usually electrical, e.g., by PD, ET or tracking

Table 2-1: Aging mechanisms and their effects

As can be seen, some mechanisms are linked to each other (e.g. thermal stress causes void formation, which will lead to PD and thus chemical byproducts in the voids). Several factors can thus be responsible for the same aging process. For paper-impregnated insulation, this therefore results in two main ways of aging that can be distinguished; thermal and electrical [4] [8].

Thermal Aging

At elevated temperatures, or if the component is overloaded, the insulation may not be able to dissipate all the energy that is generated in the conductor. Due to this increased temperature, the cellulose polymeric chains break and chemical byproducts arise, such as H₂O, CO and CO₂ [4]. The result will be a lower Degree of Polymerization (DP), as introduced earlier. This type of degradation is referred to as thermal aging.

Since H₂O is a conductive liquid, it is the most dangerous byproduct that originates during this chemical process. The existence of H₂O causes the conductivity of the insulation to increase, and therefore give a rise in the conductive losses. In figure 2-11, it is shown that H₂O in the insulation has detrimental effects on the dielectric losses in function of electric field (and thus voltage).

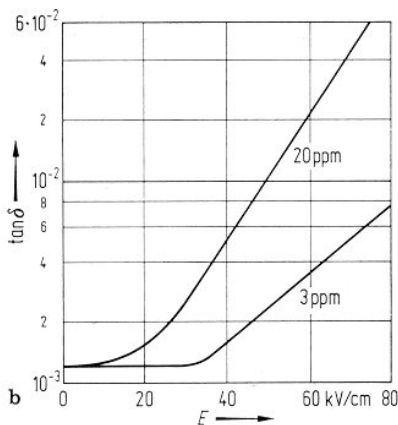


Figure 2-11: Effects of conductive liquids in the insulation on the dielectric loss tangent [9]

Secondly, the PD inception voltage (PDIV) will be lower in areas that contain these byproducts, and a local field enhancement (and thus ionization) is provided faster. Both processes (increased conductivity and faster ionization) are responsible for local overheating of the insulation. Furthermore, since the oil impregnated insulation temperature is locally enhanced, the (overheated) oil also starts to produce ethylene as a chemical byproduct and possible PD occurrence results in arcing and the origination of acetylene and ozone [4].

All these mentioned chemical byproducts that are created in the whole process of degradation find their way into the impregnated oil, either dissolved or as bubbles. Dissolved byproducts then add to the conductivity of the insulation and bubbles provide a location where PD can occur. As can be expected, this process of aging also has its influence on the temperature dependency of the dielectric losses.

Figure 2-12 shows an example of the relation between tan delta and temperature for a new (black line) and service-aged (red line) paper oil insulation.

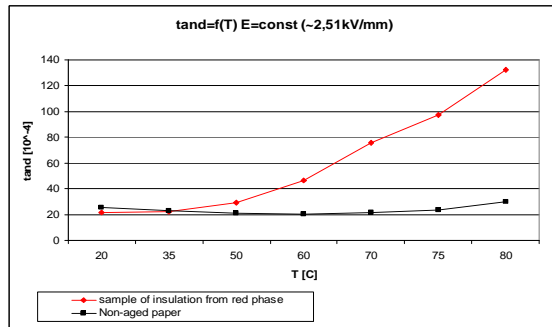


Figure 2-12: Temperature dependency of the loss tangent for new and service aged insulation [9]

As can be seen from the new insulation, the loss tangent slightly increases when the temperature rises. This phenomenon can be described by a decrease in the viscosity of the oil. This makes it easier for charge carriers to move. Because the insulation is still new, the number of pores and free spaces is limited, so no high increase is observed.

When the aged insulation is subjected to elevated temperatures, decomposition of the cellulose structure occurs (as described earlier). The byproducts that originate create more free spaces where field enhancement (and local hot spots) will originate. Due to this decomposition, and the creation of more free spaces, there are more locations available where free charge carriers can move. At elevated temperatures, when the viscosity of the oil is lower, this causes the dielectric losses to increase rapidly.

When this process starts to amplify itself, a so-called thermal runaway occurs, which leads to breakdown. Combined with that, the eventual rise in temperature also causes a smaller part of the admissible temperature rise to be available for ohmic losses in e.g. a cable, reducing its current-carrying capacity and, secondly, costs an appreciable amount of money [1].

Electrical Aging

If the electric field inside the insulation overstresses the material, the present impurities and contamination will become weak spots and gas-filled cavities can arise due to local field enhancement and partial discharges.

Inside these cavities the PD activity continues, which results in a severe erosion of the walls, and the origination of chemical byproducts as acetylene and ozone. Due to the rough structure of the walls of the cavities and the originated local field enhancement, so-called preferential areas are formed where the deterioration is more severe than in other places [10].

In the stages that follow (figure 2-13), local discharges in the preferential area will result in so-called pitting. This formation of a pit causes the breakdown strength of the insulation material to decrease because of the local degradation of the dielectric material. When the breakdown strength then falls below the existing field strength, treeing is initiated.

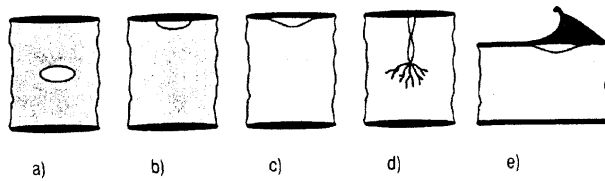


Figure 2-13: Types of defects [1]

- Internal discharges:**
 a) a void completely surrounded by the dielectric
 b) electrode-bounded cavity
 c) non-adhering electrode
 d) initiated by treeing
 e) in an interface with a longitudinal field

With the layered structure of oil impregnated insulation, and the (earlier discussed) higher field strength in the oil, it is clear that treeing occurs more easily in a radial direction (parallel to the conductor and paper-layers) [10]. As treeing is finally initiated, breakdown can occur very rapidly; between minutes to several hours.

This process of electrical aging causes the dielectric losses to increase in function of voltage, as shown in figure 2-14. This figure shows the dielectric losses for a new (black line) and service aged (red line). When concerning the new insulation, the slight increase in dielectric losses with rising voltage is caused by the porous structure of the paper insulation. In these oil-filled cavities, local field enhancements occur. As with temperature, due to the limited amount of these pores, only a small rise is visible. In the aged situation, the discharges inside the cavities are responsible for the rise in the dielectric losses. The magnitudes intensify with increasing voltage.

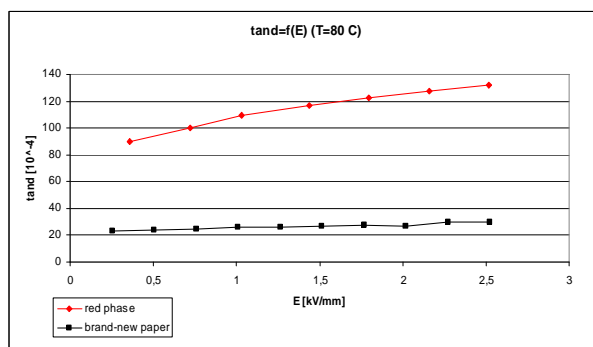


Figure 2-14: Influence of electrical aging on the dielectric losses of paper-oil insulation [9]

Finally, due to the change in chemical structure, the frequency dependency of the loss tangent changes over time.

Since the chemical structure of the insulation material changes with deterioration, also the active polarization process shift in the frequency domain. Furthermore, at lower frequencies the loss tangent increases due to increased conductivity, caused by chemical byproducts. This process is clearly visible at frequencies below 1 Hz. A well known method to examine the insulation condition with the use of frequency dependency is dielectric spectroscopy [11] [12] [13]. This method is described further in paragraph 2-3.

When examining deterioration of paper oil insulation, it is clear that not only $\tan \delta$ is an important parameter, but also $\Delta \tan \delta$ or tip-up (increase in the loss tangent as a function of temperature / voltage). In order to avoid a resulting outage and reduction in reliability of the power supply, condition monitoring on-site is of great importance.

Dielectric loss measurement is a perfect tool to investigate the current state of the insulation, and periodically measured data can be used to see whether things have worsened in time.

2.2.2 Epoxy-Mica Insulation

Insulation of stator windings suffers from gradual deterioration in time under combined electrical, thermal, mechanical and environmental stresses. The resin impregnated mica tape insulation used in electrical machines is a perfect insulator; compared to other materials it has a high thermal conductivity which makes it ideal for application in electrical machines. Generally, mica based insulation does not fail due to general aging but due to deterioration of very small defects in the insulation system itself [14].

In this section, the most frequently encountered types of defects are covered, followed by the deterioration process in epoxy-mica insulation from electrical machines.

2.2.2.1 Insulation structure [14]

The insulation of a stator can be subdivided into two sections;

- Bar-section: contains all the stator bars
- End-winding: contains the connections between the bars

Since the electric field strength is at its highest in these bar sections, this is the most interesting part for high-voltage engineering. This however does not mean that no PD occurs at the end-windings; only the probability will be much lower.

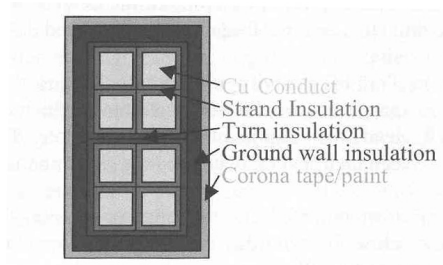


Figure 2-15:
Stator bar insulation system design [14]

Figure 2-15 shows an example of a stator bar insulation system design. As can be seen, several types of insulation are present. The so-called ground wall insulation is the most important part of this configuration, because a failure will lead to a phase-to-ground fault. When for example the strand insulation fails, only one or more turns are short-circuited. It has to be said that a defect located between two strands does cause a local hot spot, and is eventually followed by failure of the ground wall insulation.

2.2.2.2 Causes of defects

Generally, epoxy at first deteriorates with operating time, what leads to the loss of mechanical properties and delamination of the insulation. Partial discharges will then damage the whole insulation structure [15]. In stator insulation, there are several types of defect that can occur. A short overview is given hereunder [14] [16]:

- Internal voids

In stator insulation, always small voids exist. These voids are taken for granted, in order to reduce the manufacturing costs. Accepting this small PD occurrence is however not detrimental to the insulation capability. Actually, the mica in the insulation prevents the PD from developing into a complete breakdown [16]. When these voids remain small and do not significantly enlarge, the reliability of the machine is not an issue.

- Internal delamination

Internal delamination inside the insulation can be caused by imperfect curing of the insulation during manufacturing, or by mechanical or thermal over-stressing when in service. Large voids may develop that result in discharges of relatively high energy that may significantly attack the insulation. Internal delamination reduces the thermal conductivity and might lead to accelerated ageing or a thermal runaway.

- Delamination between the insulation and conductor

This type of delamination results from excessive thermal cycling and is dangerous since the turn or strand insulation can be severely damaged.

- Slot discharges

Slot discharges originate when the present coating on the conductive slots is damaged due to bar or coil movement in the slot area. This can happen due to for example erosion of the material, chemical attacks or manufacturing deficiencies. High-energy discharges will develop when serious mechanical damage is already present, which may result in additional damage to the main insulation.

- Surface discharges at end-windings

If the coating on one of the end-windings suffers from poorly designed interfaces, contamination, porosity, local heating, these types of discharges can originate. PD near the end-windings will normally occur at locations with local field enhancements.

- Conductive particles

Finally, small conductive particles in the insulation may result in a strong local concentration of PD activity.

2.2.2.3 Deterioration

Stator insulation normally fails due to the deterioration process of small defects within the material. This process that is related to the magnitude of the PD occurrence is unfortunately not well understood [17]. In the process of deterioration, the magnitude of the partial discharges shows an upward slope, but with a certain decrease every now and then (saw tooth) [14]. A picture of this process is given in figure 2-16.

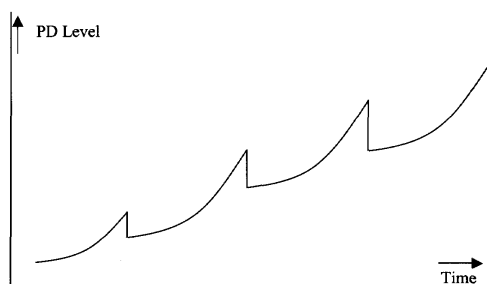


Figure 2-16: Stepwise aging of stator bar insulation [14]

In [14], a model is represented that describes this process. In that model, it is assumed that the electric tree starts from the void, but does not grow at a constant rate. When a tree reaches a barrier (e.g. a mica-flake) it will take an appreciable amount of time to get around it.

In the process that goes from a virgin cavity to an electric tree, the surface of the material is deteriorated. This surface will then become more conductive, what leads to a lower measured PD magnitude. After a certain time instant, treeing starts to develop and the

measured magnitude increases again. The repetition of this process can explain the phenomena shown in figure 2-16.

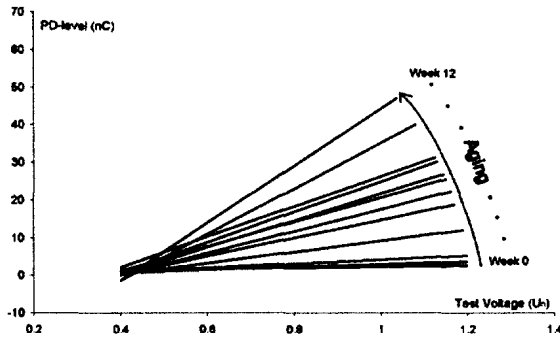


Figure 2-17: Increasing gradient shows the aging process [14]

For condition assessment, it goes without saying that this is not a preferred process. A method to determine the current state of the insulation is the voltage dependency of the PD level [14]. In figure 2-17, this relationship is shown. As the gradient of this line further increases, the aging process proceeds gradually.

2.2.2.4 Effects on $\tan \delta$

Aging in epoxy-mica insulation is caused by partial discharges that deteriorate the insulation. If many discharge sites are present at a certain moment, dielectric loss measurement can be a valuable tool.

Figure 2-18 shows the behavior of the loss tangent, as a function of voltage. It shows that from the so-called inception voltage upwards (where PD starts), the gradient of this $\tan \delta$ is much higher.

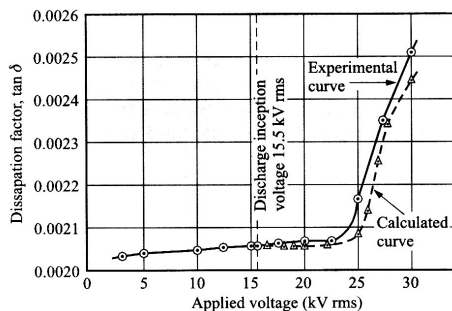


Figure 2-18: Increase in loss tangent above inception voltage PD

Since the sensitivity of this process is increased with increasing number of discharges, it will be very useful in the examination of partial discharges in machine insulation where thousands of discharges will occur simultaneously [1].

2.3 Measurement Techniques

During service conditions, high-voltage equipment suffers from aging due to electrical, thermal, environmental and mechanical stresses. These stresses will eventually cause the component to fail. In order to predict whether a cable has reached the end of its lifetime, on-site diagnosis is required. In fact, on-site diagnosis is becoming the most important non-destructive test method for HV assets e.g. cables [23].

In this chapter, several measurement techniques for determining the condition of the insulation and the measurement of the loss tangent are analyzed.

The major techniques in use for condition assessment and dielectric loss measurement are described hereunder, arranged by method of energizing the test object.

2.3.1 Continuous Energizing

2.3.1.1 Very Low Frequency Analysis

Energizing and testing component with a high capacitance (e.g. long cables) at an AC overvoltage demands reactive power of several MVA (which can impossibly be supplied by mobile installations). Therefore alternative methods are studied that are lightweight, requesting low power and are easy to transport [1].

For years, such a test object was charged with DC, but of course the physical phenomena differ from AC. One of these phenomena is the origination of space charges [10]. To avoid these DC related phenomena, nowadays VLF (Very Low Frequency) and DAC are among the used methods. VLF tests are performed with a frequency of approximately 0.1 Hz. This means that 500 times less reactive power (in case of 50 Hz) has to be supplied to the cable, and it is stressed with AC like in service.

Detection of defects with VLF can be done at a lower voltage level than with DC. Because of the low dU/dt of the VLF wave, treeing starts very slowly. Once it is started, however, it grows more rapidly than with a 50 Hz voltage. Therefore the applied VLF magnitude must exceed the service stress several times for identification of harmful insulation imperfections and the test time must be extended to an hour or longer [18,19].

2.3.1.2 The Schering Bridge

A major technique to measure a small value like $\tan \delta$ on a continuously energized cable is with a bridge circuit. A high voltage is applied to one diagonal of the bridge and a sensitive null detector is connected to the other diagonal as shown in Figure 2-19.

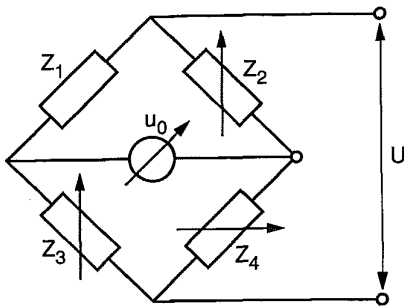


Figure 2-19: A Schering-bridge

The impedances are then adjusted in such a way, that the null detector indicates zero voltage. This is achieved when $Z_1 : Z_3 = Z_2 : Z_4$. The unknown Z_1 can then be determined using the other three values. The practical setup is given in Figure 2-20.

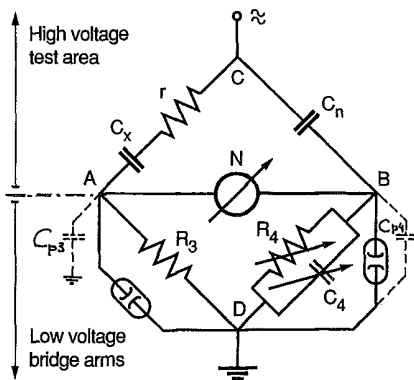


Figure 2-20: Practical setup of a Schering-bridge

Here C_n is a standard capacitor (with guard electrodes to avoid edge effects; a method for shielding of cable samples is presented in [20]) and C_x is the test object. When this bridge is balanced, the loss tangent can be obtained using [2-14].

$$\tan(\delta) = \omega R_4 C_4 \tag{2-14}$$

There are several variants of the Schering Bridge possible [1]:

- The sheaths from the coax cables that connect the high voltage bay to the bridge terminals can be brought on the same potential as the terminals itself. This is done to reduce the effect of stray capacitances.
- The bridge terminals can be brought to earth potential. This is done by bringing terminal D (earthed terminal in Figure) to a potential opposite of terminal B.
- At permanently earthed objects, the bridge principle can be reversed (earth and high potential exchanged). This means the operator has to work on high potential. This can be done by remote control or using a faraday cage that can accommodate an operator.
- For tests with unskilled operators, a differential transformer can be used instead of the usual low-voltage arm. By changing the ratios of the primary and secondary winding (using dials), the value of the capacitance and loss factor can be read instantaneously.

Finally, to check whether all stray capacitances are eliminated, [1] introduces the so-called dual balance method. By testing twice, with two different values of R_3 , the measurement errors and stray capacitances that influence the loss tangent can be determined and eliminated.

2.3.1.3 Dielectric Spectroscopy

Spectroscopy is a non-destructive method in which the dielectric condition is assessed in the frequency domain. Its principle consists on the measurement of the frequency response of both permanent and induced dipoles to the application of an external electric field. Aging causes a change in the dielectric response in the frequency domain and thus a change in the complex permittivity [11].

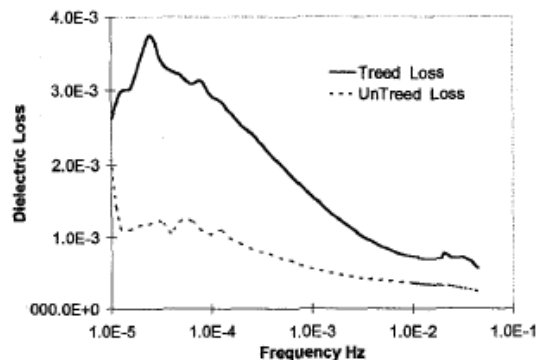


Figure 2-21: Frequency representation of the dielectric losses

Water ingress and temperature increase for example, cause a higher DC conductivity, a higher dielectric loss factor at low frequencies and a shift of the dielectric loss minimum towards higher frequencies [12]. This is illustrated in figure 2-21.

Measurement is done by a sinusoidal AC voltage, which is generated in a certain frequency range (e.g. 0.0001 – 10 Hz). The resulting current through the insulation is measured when the voltage is applied, then giving the complex impedance (capacitance, permittivity, loss tangent etc.) of the insulation [13].

2.3.2 Temporarily Energizing

2.3.2.1 Return Voltage Measurement

Return Voltage Measurement (RVM) is a non-destructive diagnostic test to determine the insulation condition. RVM is widely used for the examination of degradation in for example paper-oil cables. It works on the principle of charge displacement in the dielectric due to electrical (de)polarization. The principle is described hereunder.

A DC voltage is applied on the test object for approximately 15 minutes, in order to load it and cause charge accumulation. It is then short-circuited via an internal discharge resistor for a few seconds. If the short-circuit is cleared, a build up of a so-called return voltage occurs due to depolarization. This return voltage is very useful, because it is less sensitive to noise than other methods [21]. An example of a measurement result is given in figure 2-22.

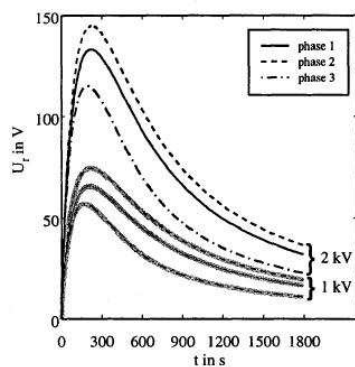


Figure 2-22: Return Voltage Characteristics of paper-oil cables

The shape of the curve (rise time, maximum voltage and relaxation time) gives information on the condition of the dielectric material. In general, aged cables are responsible for a steeper rise of the voltage curve. This effect is caused by degradation products that lead to additional conduction and polarization processes in the range of a few 10's of seconds [21].

Another change of the RVM curve is due to temperature, which also creates a shifted characteristic of the return voltage measurement [22].

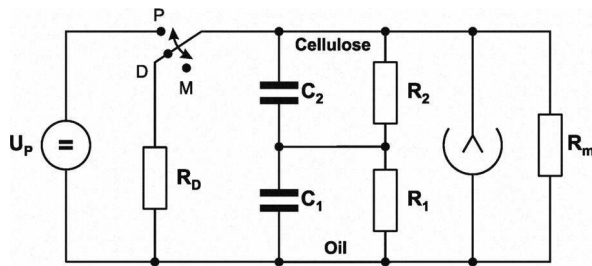


Figure 2-23: RVM Measurement Circuit

This RVM curve can be determined mathematically using a Maxwell equivalent circuit [6]. A picture of the measurement circuit for a paper-oil cable is given in figure 2-23.

$$U_r(t) = U_s \left(e^{-\frac{t}{\tau_2}} - e^{-\frac{t}{\tau_1}} \right) \quad [2-15]$$

With formula [2-15], the return voltage curve can be calculated. Here the time constants τ are given by R_1C_1 and R_2C_2 respectively. The voltage U_s is the voltage across the RC-elements after releasing the short circuit. The time constants do not change with the length of a cable, because capacitance increases and resistance decreases as a function of length [21].

2.3.2.2 Damped AC

The damped AC method makes use of a linear charging current, after which the capacitive component oscillates with an air core inductor, and therefore no reactive power is necessary. This is an important factor, because it drastically reduces the size of the test equipment.

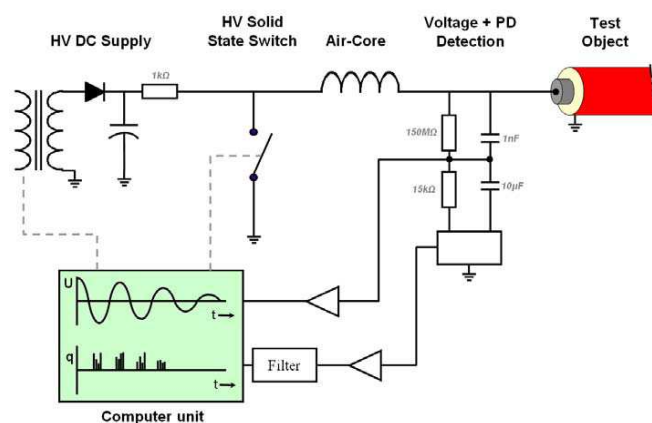


Figure 2-24: The Oscillating Wave Test System (OWTS)

A system that uses DAC voltages to detect PD and measure dielectric losses is the Oscillating Wave Test System® (OWTS). A schematic overview of this system is given in figure 2-24.

For the generation of DAC voltages, a capacitive load (the test object) is first charged with a DC power supply. After charging, the capacitive load is directly switched in series with an external inductor [23]. The resulting graph of this process is given in figure 2-25.

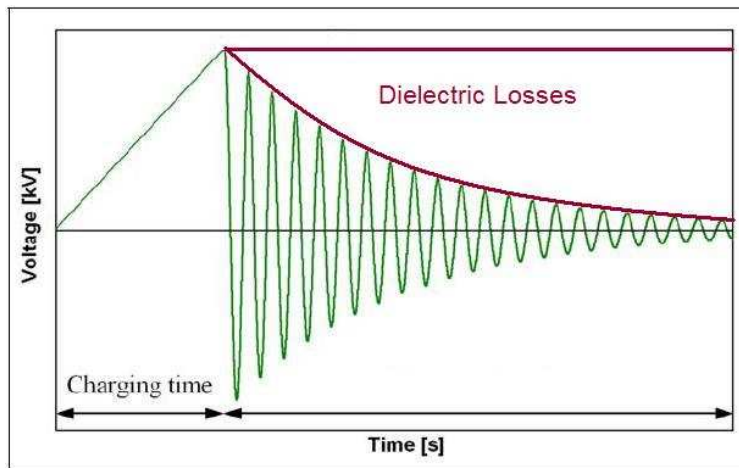


Figure 2-25: Charging and oscillation of a DAC voltage wave; the attenuation is a measure for the dielectric losses

The originated voltage wave can be simply described by formula 2-16. Here, the attenuation coefficient β is responsible for the decay of the wave and therefore a measure for the dielectric losses in the test object.

$$U(t) = e^{-\beta \cdot t} \sin(\omega \cdot t + \varphi) \quad [2-16]$$

A complete mathematical relation between the attenuation coefficient and the dielectric loss tangent is derived in the next chapter.

Frequency Variation during Condition Assessment

In practical applications, the losses are often measured around 0.1 Hz (VLF), 50 Hz (grid frequency) or several hundreds of Hz (DAC). Since it is shown earlier that these losses are frequency dependent, it is of interest whether it makes sense to measure losses at a different frequency than the one normally applied in the grid.

In practice, when a healthy dielectric is taken, the conductivity is very low. It is furthermore noticeable, that the dielectric constant (real and imaginary part) is however slowly declining in theory, but will be more or less stable (up to 1 kHz) in reality (due to the overlay of all processes).

Below, two examples that compare damped AC with 50 Hz testing are given. In figure 2-25, results from two measurements are given, that are performed with the use of DAC (high frequency) and AC (50 Hz). It can be seen, that dielectric loss measurement using damped AC voltages is a very useful tool that gives reliable results when compared to a measurement performed at 50 Hz.

Example 1			Example 2		
C=0.137uF	Tan delta measurement [%]		C=0.049uF	Tan delta measurement [%]	
Voltage	292Hz DAC	50Hz AC	Voltage	490Hz DAC	50Hz AC
0.4Un	3.10	3.0	0.4Un	3.7	3.3
0.6Un	3.11	3.0	0.6Un	3.73	3.3
0.8Un	3.11	3.1	0.8Un	3.82	3.4
1.0Un	3.12	3.2	1.0Un	3.89	4.2

Figure 2-25: an example of two measurements, both performed with DAC and AC

It is thus definitely sensible to measure at a frequency that differs from the one used in the power grid, in order to obtain a clear picture on the condition of the dielectric.

3. DAMPED AC VOLTAGES

3.1 Principle of Electrical Resonance

An inductor and a capacitor are well known energy storage elements in Electrical Engineering. An inductor stores its energy in the induced magnetic field, a capacitor in the electric field between the electrodes.

If the inductor and capacitor are connected to form an electric circuit, it is called an LC network (or RLC in case a resistance is present). Because the voltage (series circuit) and current (parallel circuit) can be described by a second order differential equation, the network is said to be of second order.

The storage elements can be described in terms of a frequency dependent reactance [3-1], [3-2].

$$X_L = 2\pi fL \quad [3-1]$$

$$X_C = \frac{1}{2\pi fC} \quad [3-2]$$

When these reactances are equal, a so-called resonance occurs. A repeating exchange between the stored energy in the magnetic field [3-3] and the stored energy in the electric field [3-4] of respectively the inductor and capacitor cause the voltage and current to oscillate.

$$W_L = \frac{1}{2} Li^2 \quad [3-3]$$

$$W_C = \frac{1}{2} Cv^2 \quad [3-4]$$

The frequency of oscillation is the resonance frequency, and can be derived from [3-5].

$$X_L = X_C \Rightarrow f_0 = \frac{1}{2\pi\sqrt{LC}} \quad [3-5]$$

3.1.1 Modelling a series RLC-circuit

3.1.1.1 Mathematical Derivation

This section is devoted to the modelling of a standard series RLC circuit. Figure 3-1 shows the representation of a series RLC-network, without a driving voltage (passive) included.

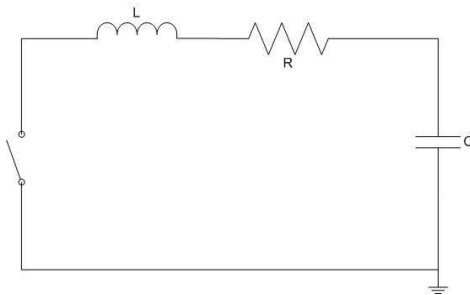


Figure 3-1: A model of a series RLC circuit, where L is the inductance in Henry's, R equals the resistance in Ohms and C represents the capacitance in Farad.

Kirchhoff's voltage law states, that the sum of all voltages in a loop of an electric circuit equals zero [3-6]. With this information, a differential equation for this network can be derived [3-7]. This derivation hereunder, which is generally known, is given in a wide variety of literature, among others [24] [25] [26],

$$V_L + V_R + V_C = 0 \quad [3-6]$$

This equation can be written as

$$L \frac{di}{dt} + Ri + \frac{1}{C} \int_{-\infty}^t i dt =$$

$$L \frac{d^2Q}{dt^2} + R \frac{dQ}{dt} + \frac{1}{C} Q = \quad [3-7]$$

$$\frac{d^2Q}{dt^2} + \frac{R}{L} \frac{dQ}{dt} + \frac{1}{LC} Q = 0$$

with current defined as the derivative of charge Q [3-8].

$$i = \frac{dQ}{dt} \quad [3-8]$$

To solve the derived differential equation, it can be written in terms of a so-called characteristic equation [3-9].

$$\lambda^2 + \frac{R}{L}\lambda + \frac{1}{LC} = 0 \quad [3-9]$$

$$\lambda^2 + 2\zeta\omega_0\lambda + \omega_0^2 = 0$$

The roots of this equation can be calculated using the quadratic equation [3-10], [3-11].

$$x = \frac{-b \pm \sqrt{b^2 - 4ac}}{2a} \quad [3-10]$$

$$x = \frac{-2\zeta\omega_0 \pm \sqrt{(2\zeta\omega_0)^2 - 4\omega_0^2}}{2} = -\omega_0\zeta \pm \omega_0\sqrt{\zeta^2 - 1} \quad [3-11]$$

This variable ζ is called the damping ratio. When this ζ is between 0 and 1, the system has complex poles $(-\omega_0\zeta \pm j(\omega_0\sqrt{1-\zeta^2}))$, and is so-called under-damped. This means an oscillation occurs which gradually diminishes.

Since $j = \sqrt{-1}$, the solution x can also be written as: $x = -\omega_0\zeta \pm \omega_0\sqrt{1-\zeta^2}$.

The solution of the differential equation then becomes (using Euler's Formula),

$$X(t) = e^{-\omega_0\zeta t} \{ \cos(\omega_0\sqrt{1-\zeta^2}t + \theta) + \sin(\omega_0\sqrt{1-\zeta^2}t + \theta) \} = \quad [3-12]$$

$$X(t) = e^{-\beta t} \{ \cos(\omega_D t + \theta) + \sin(\omega_D t + \theta) \}$$

Or, written as a function of voltage across the test object,

$$U(t) = e^{-\beta t} \{ \cos(\omega_D t + \theta) + \sin(\omega_D t + \theta) \} \quad [3-13]$$

A more detailed derivation of formulas [3-9] to [3-12] can be found in literature.

3.1.1.2 Attenuation β and Quality factor Q

As can be seen in formula [3-13], the system oscillates and is damped exponentially. The speed of this exponential damping is determined by the attenuation β , which is the product of the damping factor ζ and the resonance frequency ω_0 . For a series circuit, the attenuation is determined by [3-14].

$$\beta = \frac{R_L}{2L} \quad [3-14]$$

The quality factor Q of a series resonant circuit is the ratio of the energy stored to the energy lost in equal intervals of time [26]. The higher the quality factor is, the longer it takes for the oscillation to vanish. The quality factor equals [3-15].

$$Q = 2\pi \cdot \frac{\text{Energy Stored}}{\text{Energy dissipated per cycle}} \quad [3-15]$$

The energy stored in a resonant circuit is represented by [3-3], whereas the energy lost per cycle is given in terms of [3-16].

$$W_R = \frac{1}{2} I^2 R \cdot T = \frac{1}{2} I^2 R \left(\frac{1}{f_0} \right) \quad [3-16]$$

The quality factor for a series resonant circuit then becomes,

$$Q = \frac{X_L}{R} = \frac{X_C}{R} = \frac{1}{R} \sqrt{\frac{L}{C}} = \tan \varphi = \frac{1}{\tan \delta} \quad [3-17]$$

The angle φ represents the power factor angle and, as seen in [3-17], the quality factor is thus the reciprocal of the dielectric loss tangent. Furthermore, the square root of L/C is known as the characteristic impedance of the circuit.

3.2 A Mathematical Model of a DAC System

A damped AC system uses the principle of electrical resonance, to measure partial discharges and determine dielectric losses. Its general topology is in principle a series RLC circuit. Figure 3-2 shows a circuit model for this DAC system. This model is only valid for one frequency at a time.

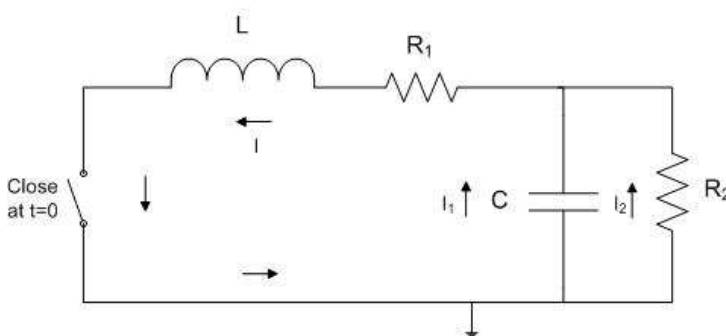


Figure 3-2: DAC-Model

In this model, R_1 represents the total internal resistance of the system, whereas R_2 represents the losses in the testobject. In the next section, a mathematical model is derived.

3.2.1 Mathematical Derivation

The (differential) equations that follow from KVL and KCL, and represent the circuit of figure 2-1, are the first step in this mathematical derivation. They are given in [3-18], [3-19], [3-20].

$$V_C + V_{R1} + V_L = \frac{1}{C} \int i_1 dt + R_1 i + L \frac{di}{dt} = 0 \quad [3-18]$$

$$V_C = V_{R2} \Rightarrow \frac{1}{C} \int i_1 dt = R_2 i_2 \quad [3-19]$$

$$i_1 + i_2 = i \quad [3-20]$$

Due to the complexity of calculation in the time domain, the given differential equations are transformed into the LaPlace domain. A more detailed explanation of LaPlace transforms is given in [27]. The transforms of [3-18] to [3-20] are given in respectively [3-21] to [3-23].

$$\frac{I_1(s)}{sC} + \frac{U_0}{s} + R_1 I(s) + sLI(s) = 0 \quad [3-21]$$

$$\frac{I_1(s)}{sC} + \frac{U_0}{s} = R_2 I_2(s) \Rightarrow I_2(s) = \frac{I_1(s)}{sR_2 C} + \frac{U_0}{sR_2} \quad [3-22]$$

$$I_1(s) + I_2(s) = I(s) \Rightarrow \left(1 + \frac{1}{sR_2 C}\right) I_1(s) + \frac{U_0}{sR_2} = I(s) \quad [3-23]$$

Where U_0 is the voltage on the test object at $t=0$. Equation [3-23] is then rewritten as a function of $I_1(s)$ [3-24], and is filled into equation [3-21]. The result is given in [3-25].

$$I_1(s) = \frac{I(s)}{1 + \frac{1}{sR_2 C}} - \frac{U_0}{sR_2} \cdot \frac{1}{1 + \frac{1}{sR_2 C}} \quad [3-24]$$

$$\frac{1}{sC} \cdot \frac{I(s)}{1 + \frac{1}{sR_2 C}} - \frac{1}{sC} \cdot \frac{U_0}{sR_2} \cdot \frac{1}{1 + \frac{1}{sR_2 C}} + \frac{U_0}{s} + R_1 I(s) + sLI(s) = 0 \quad [3-25]$$

In the resulting LaPlacian equation [3-25], $I(s)$ is the only variable that is still depending on s . This current is worked out of the equation, and the result is given in [3-26].

$$I(s) \cdot \left(\frac{s^2 R_2 LC + s(L + CR_1 R_2) + (R_1 + R_2)}{sCR_2 + 1} \right) = U_0 \cdot \left(\frac{-R_2 C}{sCR_2 + 1} \right) \quad [3-26]$$

The current then becomes,

$$I(s) = U_0 \cdot \frac{\frac{-R_2 C}{R_2 LC}}{s^2 + \left(\frac{L + CR_1 R_2}{R_2 LC} \right) s + \left(\frac{R_1 + R_2}{R_2 LC} \right)} \quad [3-27]$$

Since $U(s) = -I(s) \cdot (R_1 + sL)$, the voltage across the capacitor (and neighbouring resistor) can be written as [3-28].

$$U(s) = U_0 \left(\frac{s + \frac{R_1}{L}}{s^2 + \left(\frac{L + R_1 R_2 C}{R_2 LC} \right) s + \left(\frac{R_1 + R_2}{R_2 LC} \right)} \right) \quad [3-28]$$

To obtain the inverse LaPlace transform, the LaPlace integral has to be solved [27]. Due to the complexity of this operation a table of standard transformations, which have been derived in history, is often used to obtain the time-domain representations [27]. Instead of solving an astonishing integral, it now suffices to rewrite the formula into a “familiar” shape and rewrite it into the time-domain counterpart. This is done in [3-29] to [3-36].

$$U(s) = U_0 \left(\frac{s + \alpha}{(s + \beta)^2 + \omega^2} \right) \quad [3-29]$$

With,

$$\alpha = \frac{R_1}{L} \quad [3-30]$$

$$\beta = \frac{1}{2} \left(\frac{L + R_1 R_2 C}{R_2 LC} \right) \quad [3-31]$$

$$\omega = \sqrt{\left(\frac{R_1 + R_2}{R_2 LC} \right) - \left[\frac{1}{2} \left(\frac{L + R_1 R_2 C}{R_2 LC} \right) \right]^2} \quad [3-32]$$

Formula [3-15] then approaches

$$\omega = \sqrt{(\omega_0)^2 - (\beta)^2} \quad [3-33]$$

The inverse LaPlace transform of [3-29] appears to be [3-34], [3-36],

$$U(t) = U_0 \frac{\sqrt{(\alpha - \beta)^2 + \omega^2}}{\omega} \cdot e^{-\alpha t} \cdot \sin(\omega t + \varphi) \quad [3-34]$$

$$\text{With, } \varphi = \arctan\left(\frac{\omega}{\alpha - \beta}\right) \quad [3-35]$$

Formula [3-34] equals [3-36] and shows therefore great similarities with [3-13].

$$U(t) = U_0 \cdot e^{-\beta t} \left\{ \cos(\omega t) + \frac{\alpha - \beta}{\omega} \sin(\omega t) \right\} \quad [3-36]$$

Finally, the loss tangent has to be determined. This will be done by rewriting [3-31] into [3-37], and use this value for R_2 to determine $\tan \delta$ [3-38]. R_1 is obtained by a calibration of the system (chapter 5).

$$R_2 = \frac{L}{2\beta LC - R_1 C} \quad [3-37]$$

$$\tan(\delta) = \frac{1}{\omega R_2 C} \quad [3-38]$$

The attenuation factor β is determined from the measurement results. Due to the exponential damping, the value of an arbitrary peak can be calculated [3-39].

$$U_x = e^{-\beta t_x} \quad [3-39]$$

By using two peaks (e.g. peak 1 and 2), the attenuation can be calculated [3-40].

$$\frac{U_2}{U_1} = e^{-\beta(t_2 - t_1)} \Rightarrow \beta = -\frac{\ln\left(\frac{U_2}{U_1}\right)}{(t_2 - t_1)} \quad [3-40]$$

This model focuses on one single internal resistance. As can be seen, this model is easy to handle and gives a good representation of the system. In the next paragraph a more detailed model is derived, in order to see the differences between an easy and detailed model, and to verify which of both models is most suitable for use.

3.3 A More Detailed Model

The previously derived model consists of one component that represents the total internal resistance of the system. To get a clearer picture on the influence of for example all individual resistances, the internal resistance of the system can be represented in more detail. The result is a series resistance, which includes all components in the series loop, and a parallel component which represents the measurement setup. Figure 3-3 shows the model. As with the previous model, it is only valid for one frequency.

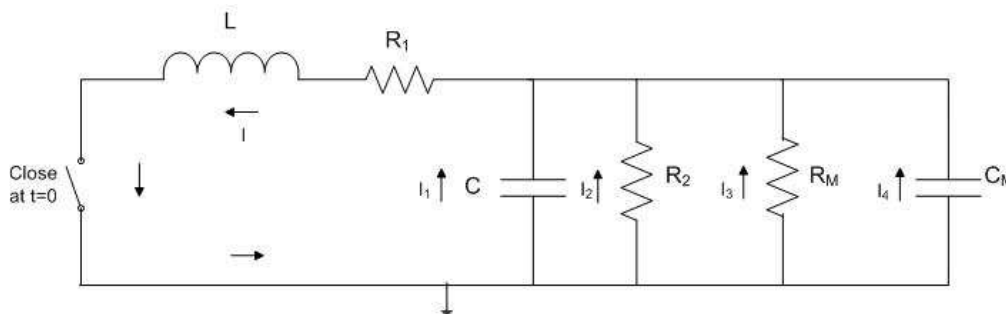


Figure 3-3: Detailed DAC model

In this model, R_1 represents the total series resistance of the primary loop, whereas R_2 represents the losses in the testobject. Furthermore, the resistive divider is represented by [3-41], and the capacitive divider by [3-42].

$$R_M = R_{HIGH-VOLTAGE ARM} + R_{LOW-VOLTAGE ARM} \quad [3-41]$$

$$C_M = \frac{C_{HV} C_{LV}}{C_{HV} + C_{LV}} \quad [3-42]$$

In the next section, a mathematical derivation of this detailed model is given.

3.3.1 Mathematical Derivation

The (differential) equations that follow from KVL and KCL, and represent the circuit of figure 3-3, are the first step in this mathematical derivation and are given in [3-43], [3-44] and [3-45].

$$V_C + V_{R1} + V_L = \frac{1}{C} \int i_1 dt + R_1 i + L \frac{di}{dt} = 0 \quad [3-43]$$

$$V_C = V_{R_2} = V_{R_M} = V_{C_M} \Rightarrow \frac{1}{C} \int i_1 dt = R_2 i_2 = R_M i_3 = \frac{1}{C_M} \int i_4 dt \quad [3-44]$$

$$i_1 + i_2 + i_3 + i_4 = i \quad [3-45]$$

Similar to the previous derivation, equations [3-43] to [3-45] are transformed into the Laplace domain and are given in respectively [3-46] to [3-50].

$$\frac{I_1(s)}{sC} + \frac{U_0}{s} + R_1 I(s) + sLI(s) = 0 \quad [3-46]$$

$$\frac{I_1(s)}{sC} + \frac{U_0}{s} = R_2 I_2(s) \Rightarrow I_2(s) = \frac{I_1(s)}{sR_2 C} + \frac{U_0}{sR_2} \quad [3-47]$$

$$\frac{I_1(s)}{sC} + \frac{U_0}{s} = R_M I_3(s) \Rightarrow I_3(s) = \frac{I_1(s)}{sR_M C} + \frac{U_0}{sR_M} \quad [3-48]$$

$$\frac{I_1(s)}{sC} + \frac{U_0}{s} = \frac{I_4(s)}{sC_M} \Rightarrow I_4(s) = \frac{I_1(s) \cdot C_M}{C} + U_0 C_M \quad [3-49]$$

$$I_1(s) + I_2(s) + I_3(s) + I_4(s) = I(s) \Rightarrow$$

$$I(s) = \left(1 + \frac{1}{sR_2 C} + \frac{1}{sR_M C} + \frac{C_M}{C} \right) I_1(s) + U_0 \left(\frac{1}{sR_2} + \frac{1}{sR_M} + C_M \right) \quad [3-50]$$

With U_0 as the voltage on the test object at $t=0$. Equation [3-50] is then rewritten as a function of $I(s)$ [3-51], and is filled into equation [3-46]. The result is given in [3-52].

$$I_1(s) = \frac{I(s)}{\left(1 + \frac{1}{sR_2 C} + \frac{1}{sR_M C} + \frac{C_M}{C} \right)} - \frac{\left(1 + \frac{1}{sR_2} + \frac{1}{sR_M} + C_M \right) \cdot U_0}{\left(1 + \frac{1}{sR_2 C} + \frac{1}{sR_M C} + \frac{C_M}{C} \right)} \Rightarrow$$

$$= \frac{(R_2 R_M C)s}{(R_2 R_M C + R_2 R_M C_M)s + (R_2 + R_M)} I(s) - \frac{(R_2 R_M C C_M)s + (R_M C + R_2 C)}{(R_2 R_M C + R_2 R_M C_M)s + (R_2 + R_M)} U_0 \quad [3-51]$$

$$\frac{1}{sC} \cdot \left(\frac{(R_2 R_M C) s}{(R_2 R_M C + R_2 R_M C_M) s + (R_2 + R_M)} I(s) - \frac{(R_2 R_M C C_M) s + (R_M C + R_2 C)}{(R_2 R_M C + R_2 R_M C_M) s + (R_2 + R_M)} U_0 \right) + \frac{U_0}{s} + R_1 I(s) + sLI(s) = 0 \quad [3-52]$$

Equation [3-52] is then rewritten into [3-53],

$$I(s) = U_0 \cdot \frac{-C}{(LC + LC_M)} \frac{1}{s^2 + \left(\frac{R_1 R_2 R_M C + R_1 R_2 R_M C_M + LR_2 + LR_M}{R_2 R_M LC + R_2 R_M LC_M} \right) s + \left(\frac{R_1 R_2 + R_1 R_M + R_2 R_M}{R_2 R_M LC + R_2 R_M LC_M} \right)} \quad [3-53]$$

Since $U(s) = -I(s) \cdot (R_1 + sL)$, the voltage across the capacitor (and neighbouring resistor) can be written as [3-54].

$$U(s) = U_0 \cdot \left(\frac{\frac{C}{C + C_M} \left(s + \frac{R_1}{L} \right)}{s^2 + \left(\frac{R_1 R_2 R_M C + R_1 R_2 R_M C_M + LR_2 + LR_M}{R_2 R_M LC + R_2 R_M LC_M} \right) s + \left(\frac{R_1 R_2 + R_1 R_M + R_2 R_M}{R_2 R_M LC + R_2 R_M LC_M} \right)} \right) \quad [3-54]$$

The inverse Laplace transform is obtained by writing [3-54] into a familiar shape [3-55].

$$U(s) = \left[U_0 \cdot \left(\frac{C}{C + C_M} \right) \right] \left[\frac{s + \alpha}{(s + \beta)^2 + \omega^2} \right] \quad [3-55]$$

With,

$$\alpha = \frac{R_1}{L} \quad [3-56]$$

$$\beta = \frac{1}{2} \left(\frac{R_1 R_2 R_M C + R_1 R_2 R_M C_M + LR_2 + LR_M}{R_2 R_M LC + R_2 R_M LC_M} \right) \quad [3-57]$$

$$\omega = \sqrt{\left(\frac{R_1 R_2 + R_1 R_M + R_2 R_M}{R_2 R_M LC + R_2 R_M LC_M} \right) - \left(\frac{1}{2} \left[\frac{R_1 R_2 R_M C + R_1 R_2 R_M C_M + LR_2 + LR_M}{R_2 R_M LC + R_2 R_M LC_M} \right] \right)^2} \quad [3-58]$$

The inverse LaPlace transform of [3-55] appears to be [3-59], [3-61],

$$U(t) = \left[U_0 \cdot \left(\frac{C}{C + C_M} \right) \right] \frac{\sqrt{(\alpha - \beta)^2 + \omega^2}}{\omega} \cdot e^{-\alpha t} \cdot \sin(\omega t + \varphi) \quad [3-59]$$

$$\text{With, } \varphi = \arctan\left(\frac{\omega}{\alpha - \beta}\right) \quad [3-60]$$

$$U(t) = \left[U_0 \left(\frac{C}{C + C_M} \right) \right] e^{-\beta t} \left\{ \cos(\omega t) + \frac{\alpha - \beta}{\omega} \sin(\omega t) \right\} \quad [3-61]$$

As with the previous derivation, the loss tangent has to be determined. The results are shown hereunder.

$$R_2 = \frac{LR_M}{2\beta R_M L(C + C_M) - R_1 R_M (C + C_M) - L} \quad [3-62]$$

$$\tan(\delta) = \frac{1}{\omega R_2 C} \quad [3-63]$$

The attenuation factor β is determined from the measurement results, and two peaks or lows can be used to calculate it.

When R_M is removed from formula [3-62] by means of dividing, a factor $\frac{L}{R_M}$ is left in the denominator. This factor vanishes if R_M approaches infinity. In practice, its value approaches gigaohms and leads to a negligible value that is extracted in the denominator of R_2 .

It can therefore be concluded, that the simplified model of section 3.2 can perfectly be used as a first approach, also because the models are only valid for one frequency and one voltage. This would unnecessarily lead to an extensive component calibration.

4. LOSS CALCULATION USING DAC

4.1 Introduction to Attenuation Coefficient β

A damped AC voltage wave can be described by the product of a sine (or cosine) wave and an exponential decay, according to [2-16], and repeated in [4-1]. In this mathematical presentation, the attenuation coefficient is a measure for the losses in the system. The loss calculation will therefore be based on this one key variable, the attenuation coefficient β .

$$U(t) = e^{-\beta t} \sin(\omega \cdot t + \varphi) \tag{4-1}$$

In general, two peaks (positive and or negative) are taken from the measured voltage wave. Combined with the corresponding time instants, it will lead to a value for the attenuation coefficient. This was mathematically shown in formula [3-40], and repeated in [4-2].

$$\frac{U_2}{U_1} = e^{-\beta(t_2-t_1)} \Rightarrow \beta = -\frac{\ln\left(\frac{U_2}{U_1}\right)}{(t_2-t_1)} \tag{4-2}$$

For clarity reasons, figure 4-1 shows a DAC wave where every peak and low is numbered. This numbering will be used throughout this chapter. When the test object is charged with positive polarity, this figure can be seen as its mirror image.

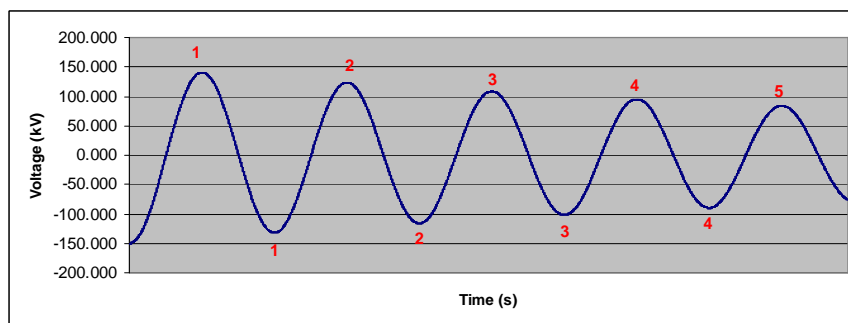


Figure 4-1: An artificial DAC voltage wave

The obtained value for the attenuation coefficient, together with the total equivalent internal resistance R_1 (see next chapter), oscillating frequency ω and inductance L will lead to a value for the dielectric losses in the capacitive test object (according to eq. [4-3]).

$$DL = \frac{2\beta}{\omega} - \frac{R_1}{\omega L} \quad [4-3]$$

In this chapter, an analysis is done on this attenuation coefficient, and a new (and more stable) method of calculation is developed. This evidence-based method will be a foundation for a more constant determination of the dielectric losses.

4.2 The Different Calculation Methods

4.2.1 Theoretical Approach

In theory, the calculation of the attenuation coefficient β is independent of which peak and/or low is taken. This is proven with a simple example.

Figure 4-2 shows a theoretical (and therefore perfect) damped AC voltage wave that is created with the help of a computer simulation program. The attenuation coefficient is chosen to be 8. For visibility reasons, the time axis is not plotted.

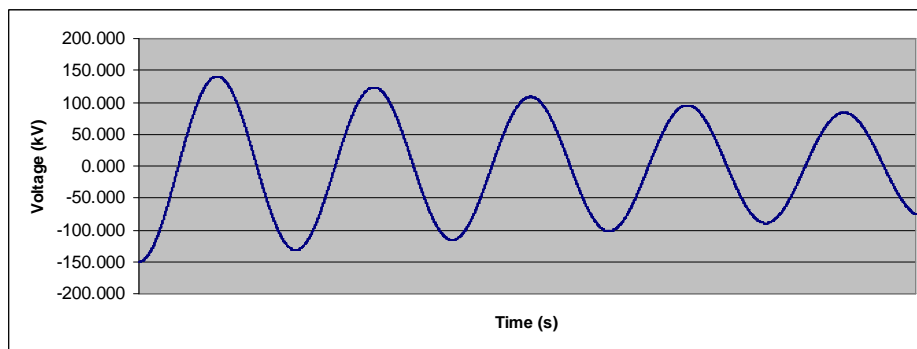


Figure 4-2: An artificial DAC voltage wave

From this data, the attenuation coefficient can now be recalculated (formula [4-2]) and should be 8, independent of the choice of peaks and/or lows. Tables 4-1 to 4-3 show the calculation of β respectively as a function of peaks, lows and combinations of both.

The first column consists of the first peak/low taken and the first row consists of the second peak/low involved.

peak peak	1	2	3	4
1		8.005	8.002	8.001
2			7.999	7.999
3				7.999
4				

Table 4-1: Attenuation as a function of peaks

low low	1	2	3	4
1		8.013	8.006	8.004
2			7.999	7.999
3				7.999
4				

Table 4-2: Attenuation as a function of lows

peak \ low	1	2	3	4
1	8.02	8.01	8.00	8.00
2	8.01	8.01	7.99	8.00
3	8.01	8.00	8.01	7.99
4	8.00	8.00	8.00	8.01

Table 4-3: Attenuation as a function of peaks and lows combined

To make this example as realistic as possible, a comparable time step is taken as in a real DAC system. Except small errors (due to the time step taken and determination of the minimum value of the starting low), all values are approximately 8.

In practice however, this is not always as clear as shown in this example. In the next section, the attenuation coefficient of measurement data from the field is analyzed.

4.2.2 Attenuation in Practice

To draw conclusions on the determination of β , a vital part will be the analysis of measurement data from the field. Because the theoretical approach showed a constant value in all situations, tables were used to present this outcome. In this practical approach, figures are used to visualize the differences between the chosen methods of calculation.

Figure 4-3 shows the attenuation as a function of different peaks during a test with 120 kV on a 120 kV cable. On the right (the legend), the first peak is given, the second used peak can be found on the x-axis. This cable was charged with positive polarity.

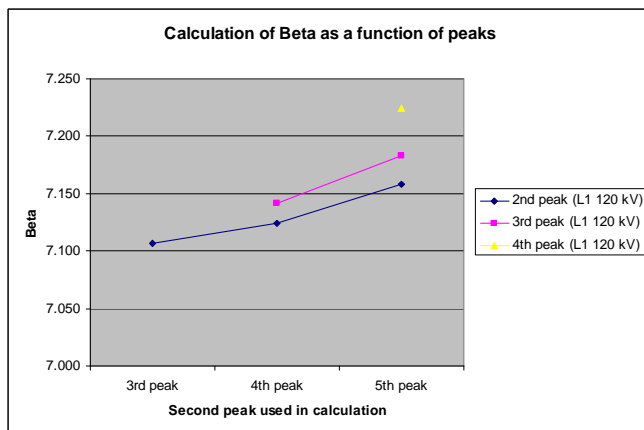


Figure 4-3: Attenuation as a function of peaks of a 120 kV oil impregnated cable in a 120 kV test. The total cable length is 5300 meters

From the same measurement, the results for different lows and combinations of peaks and lows are calculated. These results are shown in figure 4-4 and 4-5. For comparing reasons, the scaling is kept constant.

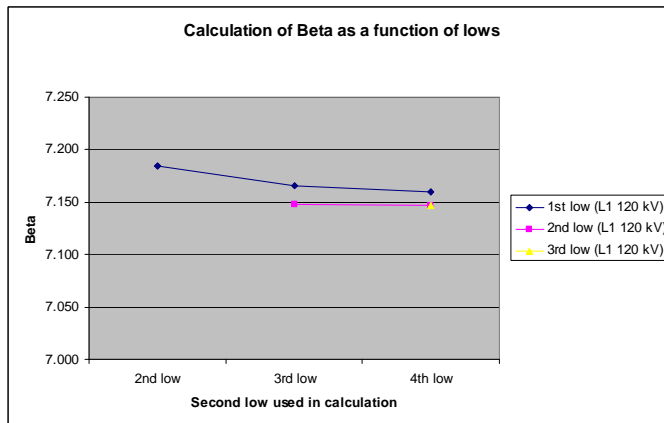


Figure 4-4: Attenuation as a function of lows of a 120 kV oil impregnated cable in a 120 kV test. The total cable length is 5300 meters

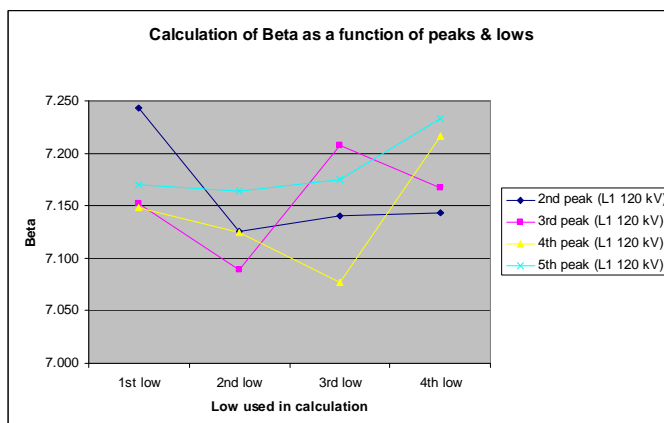


Figure 4-5: Attenuation as a function of peaks and lows of a 120 kV oil impregnated cable in a 120 kV test. The total cable length is 5300 meters

The outcome of this particular measurement is representative for the large amount of data that is analyzed during this research.

This is further shown in a second example, where the same figures are presented as in 4-3 to 4-5. This example includes a measurement at 150 kV, on an XLPE cable (nominal voltage 130 kV) with a total length of 2200 meters.

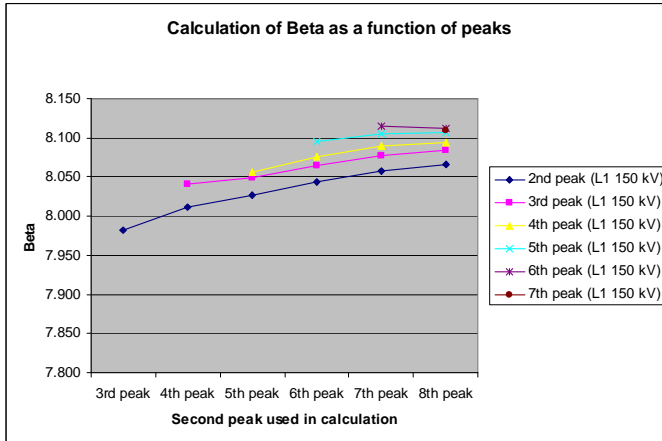


Figure 4-6: Attenuation as a function of peaks of a 130 kV XLPE cable in a 150 kV test. The total cable length is 2200 meters

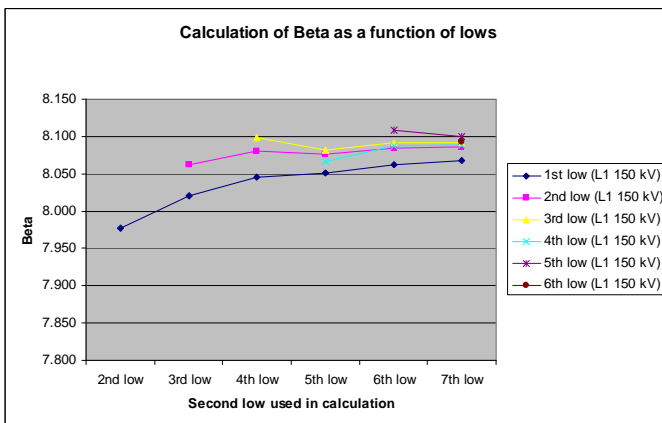


Figure 4-7: Attenuation as a function of lows of a 130 kV XLPE cable in a 150 kV test. The total cable length is 2200 meters

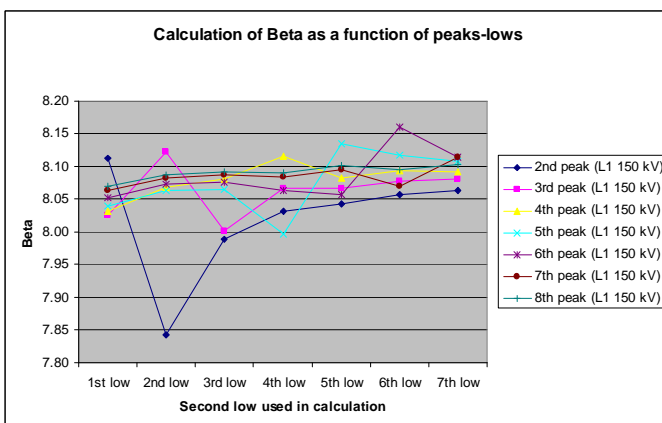


Figure 4-8: Attenuation as a function of peaks and lows combined, of a 130 kV XLPE cable in a 150 kV test. The total cable length is 2200 meters

On the analysis done on the attenuation coefficient, in function of peaks / lows and a combination of both, several observations can be made. An overview of the major visibilities is presented hereunder.

- The attenuation coefficient as a function of peaks and lows combined behaves very unstable. This is a general observation that is valid for all data analyzed.
- The calculation from only peaks (or only lows) is more constant, but sometimes slowly increases or declines with every succeeding oscillation.
- The obtained value for the attenuation coefficient from two peaks is not always exactly the same as from two lows. This can probably explain the unstable behavior of peak-low calculation.

The observations that are made show the importance of which two peaks and/or lows are taken in the calculation of attenuation coefficient β .

From the fact that the calculation of the attenuation from one peak and one low is very unstable, it can be concluded that most likely some sort of offset is present in the measured data. The investigation on this issue is continued in the next paragraph, with an analysis on the effects of an offset on the obtained value for β .

4.3 Including an Offset

4.3.1 Introduction

An offset is generally defined as a shift of the measured voltage wave when earth potential is its reference. This difference between the virtual and real earth can be the result of different events and occurrences. A few major ones are listed hereunder.

- Grounding of the system, this contains sufficient impedance and will consequently lead to a voltage drop.
- Inaccuracy of the measurement setup (e.g. due to the chosen sample frequency for the voltage wave), and the fact kV's are translated into volts before being processed further.

This paragraph starts with a theoretical investigation on the effects of an offset on the calculation of the attenuation coefficient. It is assumed that the offset is in majority constant. Four experiments are performed; a positive offset of 1 and 10 kV (extreme value, for ease of interpretation), and a negative offset of 1 and 10 kV. For this analysis, the theoretical voltage wave from section 4.1 is used. To be as realistic as possible, again the same sample frequency as in reality is used for this wave.

4.3.2 Positive Offset

4.3.2.1 A small offset

The first investigation focuses on a positive offset of 1 kV. The voltage wave is shifted upwards, and the attenuation coefficient is calculated. The results are presented in tables 4-4 to 4-6.

peak peak	1	2	3	4
1		7.945	7.938	7.932
2			7.931	7.926
3				7.921
4				

Table 4-4: Attenuation as a function of peaks with 1kV positive offset

low low	1	2	3	4
1		8.070	8.067	8.069
2			8.064	8.069
3				8.073
4				

Table 4-5: Attenuation as a function of lows with 1kV positive offset

peak \ low	1	2	3	4
1	6.30	9.83	8.65	8.42
2	7.40	6.06	10.07	8.74
3	7.61	7.31	5.79	10.35
4	7.70	7.55	7.21	5.49

Table 4-6: Attenuation as a function of peaks and lows combined with 1kV positive offset

4.3.2.2 An extreme value

The second test includes a (fictive) situation, when a positive offset of 10 kV is present. The results are given in tables 4-7 to 4-9.

peak peak	1	2	3	4
1		7.441	7.402	7.363
2			7.364	7.324
3				7.284
4				

Table 4-7: Attenuation as a function of peaks with 10kV positive offset

low low	1	2	3	4
1		8.627	8.665	8.714
2			8.704	8.757
3				8.810
4				

Table 4-8: Attenuation as a function of lows with 10kV positive offset

peak \ low	1	2	3	4
1	9.16	26.33	14.58	12.27
2	1.92	11.45	28.83	15.49
3	4.10	1.10	14.13	31.72
4	5.01	3.57	0.15	17.19

Table 4-9: Attenuation as a function of peaks and lows combined with 10kV positive offset

It can be seen that the larger the offset becomes, the less stable the calculation from one peak and one low combined becomes. The calculation from only peaks or lows changes, but remains more or less constant with succeeding oscillations.

The same analysis is done on a negative offset, in order to compare the results and draw solid conclusions.

4.3.3 Negative Offset

4.3.3.1 A small offset

The third simulation is with a negative offset of 1 kV. The voltage wave is shifted downwards, and the attenuation coefficient is calculated. The results are presented in tables 4-10 to 4-12.

peak peak	1	2	3	4
1		8.067	8.068	8.071
2			8.069	8.074
3				8.078
4				

Table 4-10: Attenuation as a function of peaks with -1kV negative offset

low low	1	2	3	4
1		7.956	7.946	7.939
2			7.935	7.931
3				7.926
4				

Table 4-11: Attenuation as a function of lows with -1kV negative offset

peak \ low	1	2	3	4
1	9.74	6.18	7.35	7.58
2	8.62	9.95	5.92	7.26
3	8.40	8.70	10.22	5.64
4	8.31	8.45	8.79	10.53

Table 4-12: Attenuation as a function of peaks and lows combined with -1kV negative offset

4.3.3.2 An extreme value

The final test includes a (fictive) situation again, when a negative offset of 10 kV is present. The results are shown in tables 4-13 to 4-15.

peak peak	1	2	3	4
1		8.663	8.709	8.763
2			8.755	8.812
3				8.870
4				

Table 4-13: Attenuation as a function of peaks with -10kV negative offset

low \ low	1	2	3	4
1		7.481	7.440	7.402
2			7.400	7.363
3				7.325
4				

Table 4-14: Attenuation as a function of lows with -10kV negative offset

peak \ low	1	2	3	4
1	25.28	10.23	1.52	3.85
2	14.18	27.56	12.73	0.64
3	12.01	15.02	30.27	15.59
4	11.11	12.56	16.00	33.36

Table 4-15: Attenuation as a function of peaks and lows combined with -10kV negative offset

4.3.4 Observations

From the analysis on the influence of an offset, some observations can be made. These observations are listed below.

- When a positive offset is present, the attenuation coefficient that is determined from two peaks declines, whereas the value calculated from two lows increases. With a negative offset, this will be the other way around.
- Although these values decline or increase, its value in function of succeeding peaks remains more or less constant.
- The attenuation coefficient, that is determined from one peak and one low, becomes highly unstable when an offset is present.

From the data analysis on measurements from the field, (paragraph 4.2), it is plausible that an offset is responsible for the behavior of the attenuation coefficient in function of peaks and lows.

4.4 A New Calculation Method for β

4.4.1 Introduction

To calculate the losses from a damped sine wave, the attenuation coefficient β has to be determined. As shown in the previous paragraph, an offset can be of great influence on the measurement and calculation. In order to calculate an attenuation that is most stable under different situations (voltage level, capacitance value, offset), a new method is introduced. This method uses the value for β that is calculated from the first two peaks, and averages it with β calculated from the first two lows (equation [4-4]).

$$\beta = \frac{\beta_{\text{peak1-peak2}} + \beta_{\text{low1-low2}}}{2} \quad [4-4]$$

To check the accuracy of this new calculation, a theoretically generated damped oscillation is fitted to a set of measured data with the use of computer simulation program Matlab. In this way, the attenuation coefficient of the entire oscillation can be determined with great accuracy and a comparison can be made between the current and new method. Later on, the trend line (in function of increasing test voltage) is compared.

4.4.2 Application to measurement data

The newly introduced method is applied to measurement data with different capacitance values, voltage levels and offsets. This wide variety of data will result in a solid foundation for conclusions that are drawn in paragraph 4.5.

4.4.2.1 Effects of an Offset

Voltage level 28 kV and Capacitance 0.5 uF

The first measurement that is analyzed is a 28 kV test with a test object of 0.5 uF. Table 4-16 shows the results for different offsets.

offset (kV)	peaks	lows	1st peaks	1st lows
-5.0	25.102	15.084		20.093
-3.0	23.027	16.118		19.572
-1.0	21.268	17.305		19.286
-0.5	20.870	17.629		19.249
0.0	20.486	17.966		19.226
0.5	20.116	18.316		19.216
1.0	19.759	18.680		19.220
3.0	18.451	20.293		19.372
5.0	17.304	22.211		19.758

Table 4-16: Attenuation, as a function of offset at 28 kV and 0.5 uF.

Here, column “peaks” is the calculated value from the first two peaks, column “lows” is the calculated value from the first two lows, and “1st peaks 1st lows” contains the average of both values. Figure 4-9 shows the graphical representation of table 4-16.

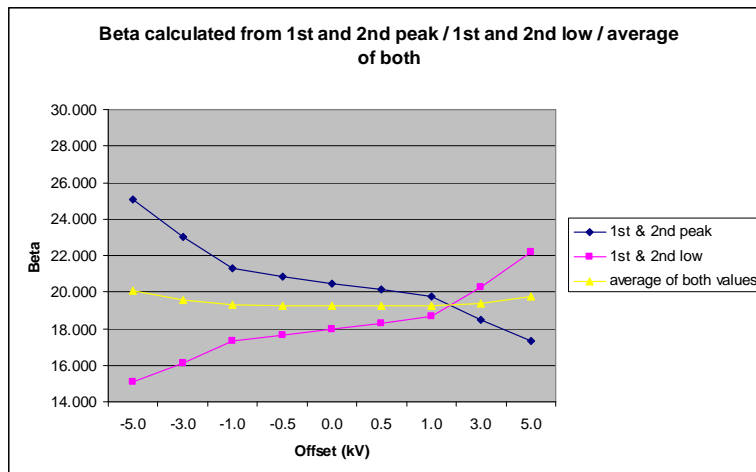


Figure 4-9: Attenuation, as a function of offset at 28 kV and 0.5 μ F.

With the use of matlab, a generated wave is fitted to the measured data. The red line (in figure 4-10) represents the measurement results, whereas the blue oscillation equals the fitted curve (only visible at $t=0$ and therefore almost perfectly fitted).

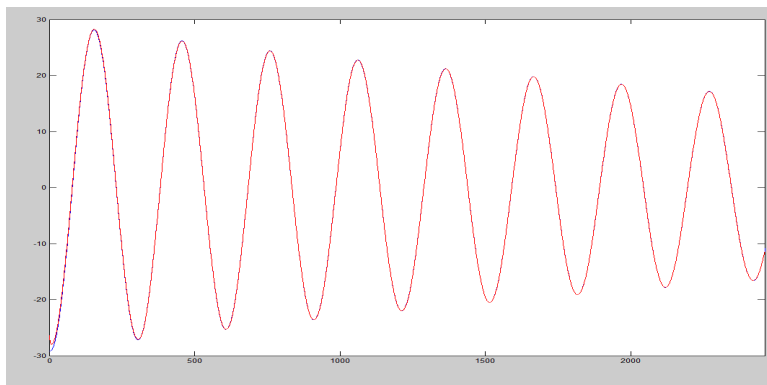


Figure 4-10: Fitted wave onto measured data (28 kV, 0.5 μ F)

The value for β that is calculated by Matlab is 18.607. This increases to 18.702 when fitted from the first zero crossing onwards. Although this value is still 0.5 below the averaged value from table 3-16, it is already an improvement compared to the (currently used) 20.486 (obtained from the first two peaks). This shows the advantage of averaging, errors can be (partially) corrected.

Voltage level 150 kV and Capacitance 0.5 uF

The second measurement that is analyzed is a 150 kV test with a test object of again 0.5 uF. The results are given in table 4-17 and figure 4-11.

offset (kV)	peaks	lows	1st peaks	1st lows
-5.0	7.843	7.275		7.559
-3.0	7.723	7.386		7.555
-1.0	7.608	7.501		7.554
-0.5	7.579	7.530		7.555
0.0	7.551	7.559		7.555
0.5	7.523	7.589		7.556
1.0	7.495	7.619		7.557
3.0	7.386	7.741		7.563
5.0	7.280	7.866		7.573

Table 4-17: Attenuation, as a function of offset at 150 kV and 0.5 uF.

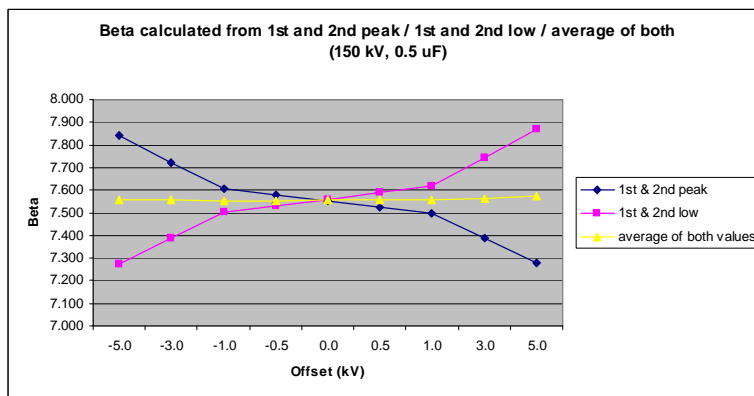


Figure 4-11: Attenuation, as a function of offset at 150 kV and 0.5 uF

The attenuation coefficient of the fitted curve is 7.566. This measurement clearly shows no offset, its calculated value is equal to the currently used number (as well as all averages).

Voltage level 28 kV & Capacitance 0.95 uF

The third measurement that is analyzed is a 28 kV test with a test object of 0.95 uF. The results are given in table 4-18 and figure 4-12.

offset (kV)	peaks	lows	1st peaks	1st lows
-5.0	21.977	14.140		18.058
-3.0	20.110	15.138		17.624
-1.0	18.536	16.288		17.412
-0.5	18.180	16.603		17.391
0.0	17.837	16.931		17.384
0.5	17.508	17.272		17.390
1.0	17.190	17.627		17.408
3.0	16.027	19.205		17.616
5.0	15.011	21.095		18.053

Table 4-18: Attenuation, as a function of offset at 28 kV and 0.95 uF.

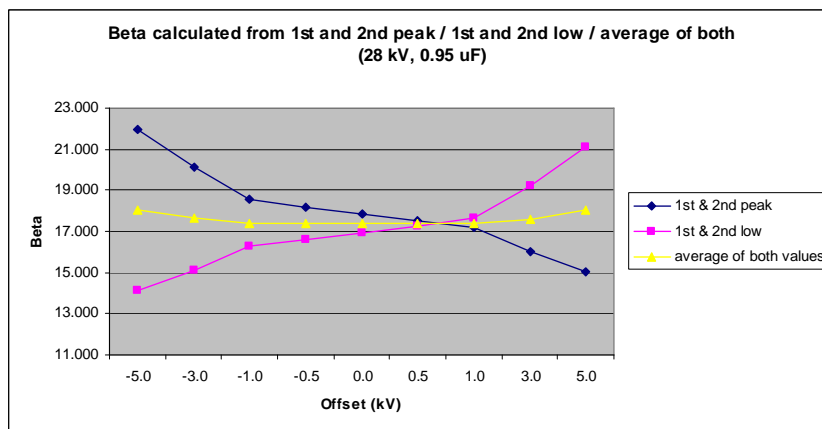


Figure 4-12: Attenuation, as a function of offset at 28 kV and 0.95 uF

The computer calculated value for the attenuation coefficient is 17.183.

Voltage level 50 kV & Capacitance 7.2 uF

The fourth measurement that is analyzed is a 50 kV test with a test object of 7.2 uF. The results are given in table 4-19 and figure 4-13.

offset (kV)	peaks	lows	1st peaks	1st lows
-5.0	10.239	7.640		8.940
-3.0	9.718	8.013		8.866
-1.0	9.247	8.425		8.836
-0.5	9.136	8.535		8.835
0.0	9.028	8.647		8.838
0.5	8.922	8.763		8.843
1.0	8.819	8.881		8.850
3.0	8.430	9.390		8.910
5.0	8.074	9.961		9.017

Table 4-19: Attenuation, as a function of offset at 50 kV and 7.2 uF.

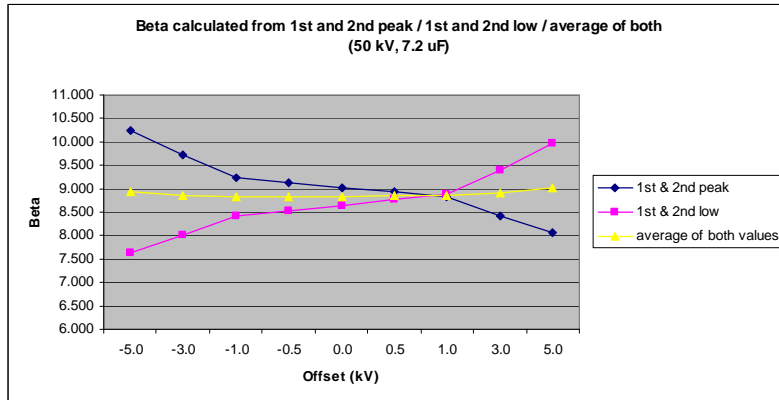


Figure 4-13: Attenuation, as a function of offset at 50 kV and 7.2 uF

In this example, the computer calculated value for the attenuation coefficient is 8.922.

Voltage level 60 kV & Capacitance 10.87 uF

The fifth and final measurement that is analyzed is a 60 kV test with a test object of 10.87 uF. The results are given in table 4-20 and figure 4-14.

offset (kV)	peaks	lows	1st peaks	1st lows
-5.0	9.767	7.677		8.722
-3.0	9.339	8.012		8.676
-1.0	8.948	8.377		8.663
-0.5	8.855	8.474		8.665
0.0	8.764	8.573		8.669
0.5	8.675	8.674		8.675
1.0	8.588	8.777		8.683
3.0	8.256	9.218		8.737
5.0	7.950	9.706		8.828

Table 4-20: Attenuation, as a function of offset at 60 kV and 10.87 uF.

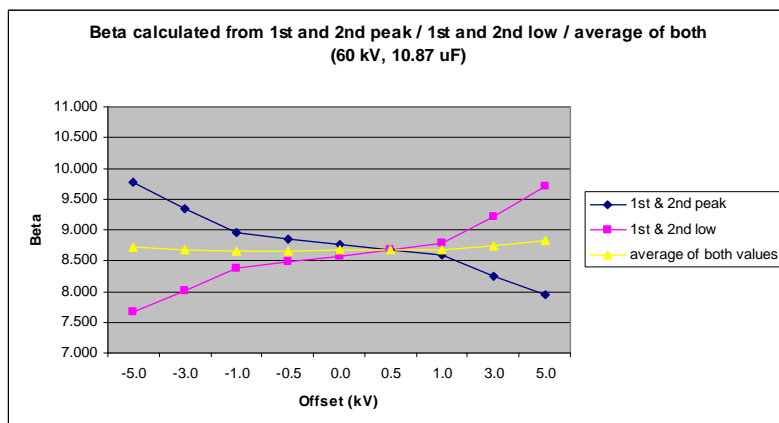


Figure 4-14: Attenuation, as a function of offset at 60 kV and 10.87 uF

The calculated value for the attenuation coefficient is 8.751.

From the results that are presented above, it can be seen that the new method of calculation eliminates the effects of an offset, and therefore increases the stability of the attenuation calculation.

The final step in the introduction of this new method is verification, and comparison of the attenuation coefficient as a function of voltage. The currently used calculation parameters for the attenuation coefficient are compared to the new calculation, and the trend line ($\Delta \tan \delta$) should be identical.

4.4.2.2 Influence on the Voltage Trendline

Voltage level 230 kV and Capacitance 4 uF

Figure 4-15 shows the voltage dependency in a 230 kV cable, as a function of the first two peaks, first two lows and the average value. The results are also presented in table 4-21.

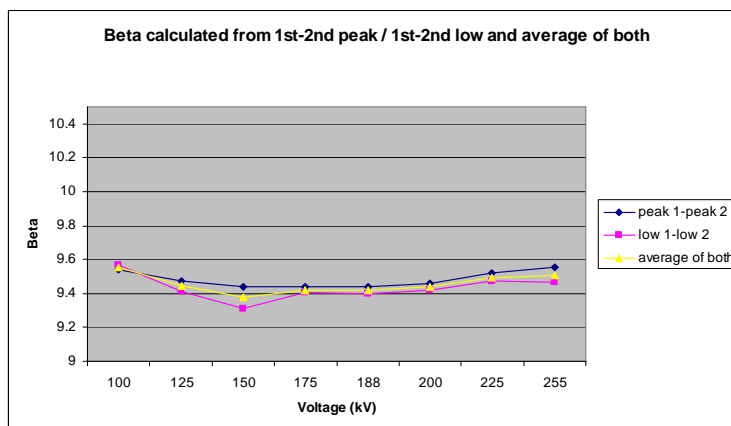


Figure 4-15: Attenuation as a function of voltage

Voltage (kV)	1st-2nd peak	1st-2nd low	Average
25	10.387	10.321	10.354
50	9.812	9.751	9.782
75	9.615	9.489	9.552
100	9.543	9.566	9.554
125	9.472	9.415	9.444
150	9.440	9.313	9.376
175	9.436	9.403	9.420
188	9.437	9.398	9.418
200	9.461	9.421	9.441
225	9.518	9.472	9.495
255	9.553	9.465	9.509

Table 4-21: Attenuation, as a function of voltage (same as figure 4-15)

As can be seen, the new calculation method gives the same results as the current commonly used first and second peak. The given result is of phase L3, but shows a similar outcome to that in L1 and L2.

Voltage level 150 kV and Capacitance 1.6 uF

The second set of data that is analyzed is from a 150 kV oil impregnated cable. The only difference with figure 4-15 is the way of charging; this cable was charged at positive polarity.

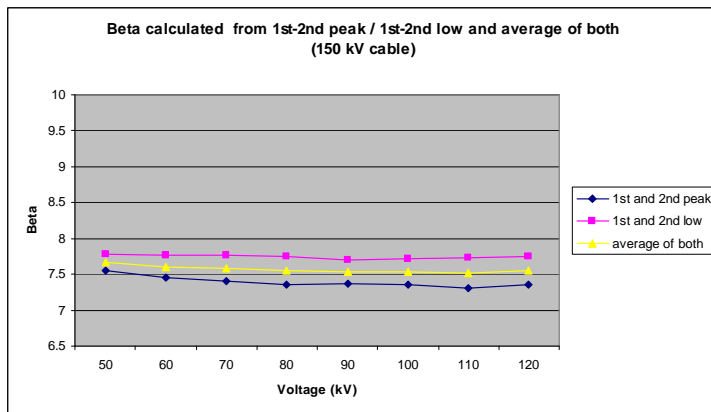


Figure 4-16: Attenuation as a function of voltage

Voltage (kV)	1st-2nd peak	1st-2nd peak	Average
10	9.107	9.345	9.226
20	8.067	8.259	8.163
30	7.719	7.954	7.836
40	7.630	7.887	7.758
50	7.553	7.784	7.668
60	7.450	7.764	7.607
70	7.404	7.769	7.587
80	7.355	7.756	7.556
90	7.379	7.696	7.538
100	7.356	7.722	7.539
110	7.310	7.728	7.519
120	7.350	7.752	7.551

Table 4-22: Attenuation, as a function of voltage (same as figure 4-3)

The same results are shown in table 4-22. As can be seen, it appears as if there is a certain offset present in this measurement (a difference between the peaks and lows). Therefore, the voltage wave at 120 kV is fitted by an artificial wave in Matlab. The attenuation coefficient is determined as 7.654, which means that the average value is among the closest values calculated.

Voltage level 150 kV and Capacitance 1 uF

The third set of data that is analyzed is from a 150 kV XLPE cable at the HV laboratory, and has a total length of 100 meters. Phase L3 shows a dielectric loss of 0.1 % up till 150 kV (calculated during the measurement, with the currently used method). Figure 4-17 shows the results as a function of voltage.

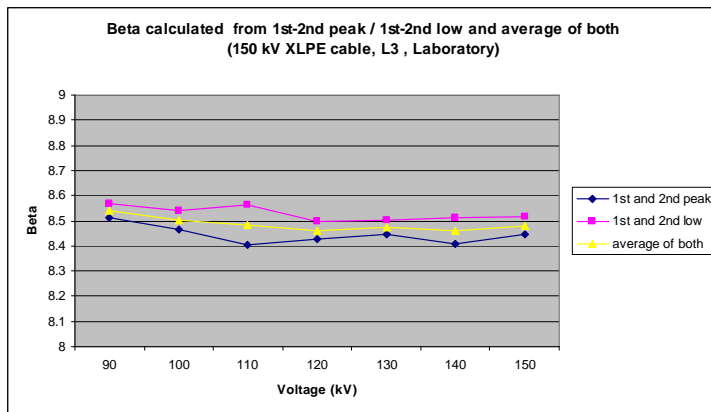


Figure 4-17: Attenuation as a function of voltage

Voltage (kV)	1st-2nd peak	1st-2nd peak	Average
40	8.843	8.952	8.897
50	8.669	8.822	8.745
60	8.606	8.729	8.668
70	8.542	8.617	8.580
80	8.509	8.572	8.541
90	8.514	8.570	8.542
100	8.462	8.538	8.500
110	8.405	8.565	8.485
120	8.429	8.496	8.462
130	8.448	8.501	8.474
140	8.408	8.511	8.459
150	8.445	8.515	8.480

Table 4-23: Attenuation, as a function of voltage (same as figure 4-17)

The results presented in this paragraph, show very similar results. In the final part of this chapter, conclusions are drawn on the data analysis.

4.5 Chapter Conclusions

From the data that is analyzed in this chapter, several observations and conclusions can be drawn. An overview is listed hereunder.

- In theory, when no offset is present, it does not matter which peaks and/or lows are taken in the calculation of β .
- The analysis on the measurement data from the field reveals, that an attenuation calculation from one peak and one low is very unstable, and suggest some sort of offset.
- An upward shift of the voltage wave (positive offset) causes the calculated attenuation of the peaks to decrease and the attenuation of the lows to increase.
- A downward shift shows the opposite, the attenuation of the peaks increases, whereas the attenuation of the lows decreases.
- The larger the offset (positive or negative), the less accurate the calculation of β using peaks and lows combined will be.
- The average value of beta calculated from the first two peaks and first two lows comes closer to the correct value (proved by an artificial wave that was fitted on the measurement data), and eliminates the effects of an offset.
- All the analyzed data, at different voltage levels, capacitance values and offsets show similar results; averaging improves and stabilizes the calculation for the attenuation coefficient.
- The fitted curves do not match well at the starting peak. To avoid edge effects and create a wave that fits the largest part of the dataset, all curves are fitted from the first zero crossing onwards, what results in a much better accuracy for the entire set of measurement data.
- When the voltage dependency of the damping is examined, the same trendline is visible when comparing the current method and the newly introduced one. This is of great importance, since $\Delta \tan \delta$ is a valuable parameter to determine the condition of the test object.

5. THE INTERNAL SYSTEM LOSSES

5.1 The Current Calibration Procedure

A damped AC system can be used to diagnose capacitive test objects (e.g. measure partial discharges and determine dielectric losses). Its topology is in principle a series RLC circuit, as shown and mathematically supported in chapter 3. Figure 5-1 shows the circuit model that is currently used to analyze the system.

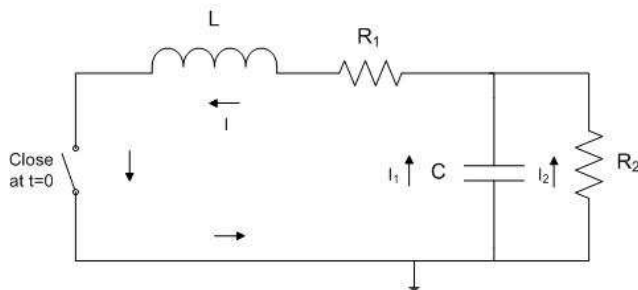


Figure 5-1: A DAC-system Model

Since the system itself will not be completely lossless in practice, R_1 represents the total internal resistance of the system, whereas R_2 represents the losses in the test object.

Due to the fact, that the internal resistance R_1 is only valid for one voltage level and one frequency, an extensive calibration procedure is necessary to determine this R_1 value at different voltages and frequencies. The result will be a matrix (with U and f on both axes) filled with values for R_1 . Figure 5-2 shows a graphical representation of such a table.

To obtain these internal resistance values, several capacitors are used. These are then successively switched in series and parallel, to vary the total capacitance (and thus the frequency) in a complete range of system voltages. Since the dielectric losses of the test capacitors are known, the internal resistances can then be calculated using equation [5-3], where R_1 will be the only unknown variable left.

During a measurement in the field, the test voltage and oscillation frequency are used to obtain a corresponding value for R_1 from the matrix. Between the calibrated data points, the numbers are bilinear interpolated. All together, it goes without saying that this whole calibration procedure is very time-consuming and elaborate.

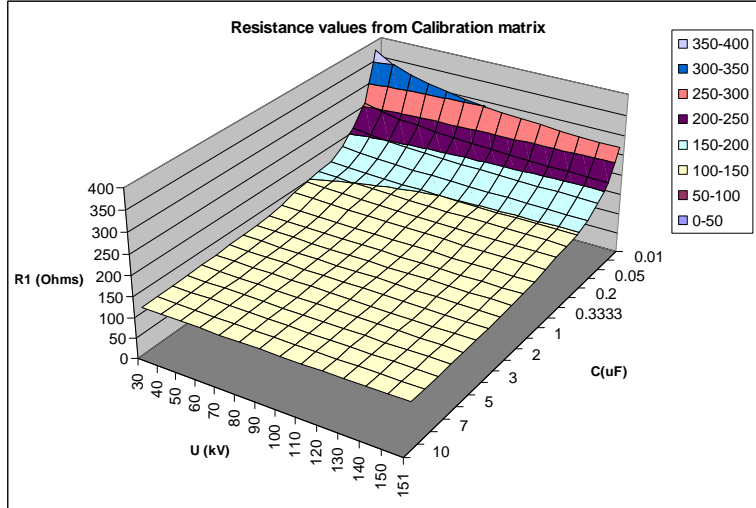


Figure 5-2: Calibration matrix given graphically

The resistance of the dielectric, and its corresponding loss tangent, are determined with the use of equation [5-1] and [5-2], as shown earlier.

$$R_2 = \frac{L}{2\beta LC - R_1 C} \quad [5-1]$$

$$\tan(\delta) = \frac{1}{\omega R_2 C} \quad [5-2]$$

Here, β is the measured attenuation, L is the inductance, C is the capacitance of the test object, R_1 is the total internal resistance of the system itself and R_2 is the resistance that represents the dielectric losses.

When these equations are entered into each other, the relation of R_1 to the dielectric losses (equation [5-3]) will be the result.

$$DL = \frac{2\beta}{\omega} - \frac{R_1}{\omega L} \quad [5-3]$$

In this chapter, it is examined whether improvement can be made on this extensive calibration method, without the loss of accuracy.

5.2 Investigation on the Calibration Matrices

5.2.1 An Experimental Approach

It is shown in paragraph 5.1, that the internal resistance values that are obtained during the calibration can represent a 3D plane, with an asymptotical behavior at decreasing capacitance values.

Due to this behavior, it is chosen to translate this capacitance axis into a frequency axis. Since a simplified calibration means, in general, less calibration points, an experimental approach is chosen where the relation between internal resistance and frequency becomes linear. The relation between frequency and capacitance is given in eq. [5-4].

$$f = \frac{1}{2\pi \cdot \sqrt{LC}} \quad [5-4]$$

Since the inductance L of a system is known, the translation can easily be made. With this mathematical operation, the square root that exists between the capacitance and frequency is eliminated.

An example is given below. Here, a 150 kV DAC system matrix is analyzed. The capacitance values at 150 kV are transformed into frequencies. The inductance is chosen to be 8.9 Henry. Although this value may be different in reality, its constant character makes it independent of the results presented hereunder. The frequency at a capacitance value of 10 uF is determined to be 16.87 Hz and this becomes 533.49 Hz at the lower border of 0.01 uF.

The results that are then obtained show a linear relation to each other. In figure 5-3, a so-called scatter plot is used to present the data on a linear scale.

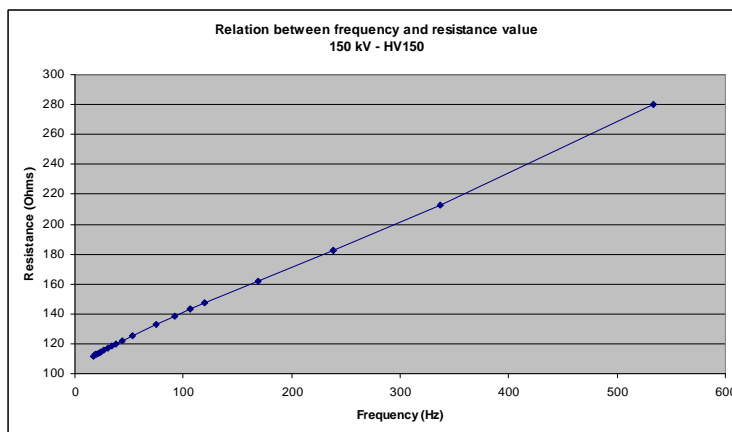


Figure 5-3: Linear relation between internal resistance and frequency at 150 kV in a 150 kV DAC system

Furthermore it appears that these linear relation remains when the test voltage of the system is varied. The only parameter that changes is the gradient of the line. This increases with lower voltages.

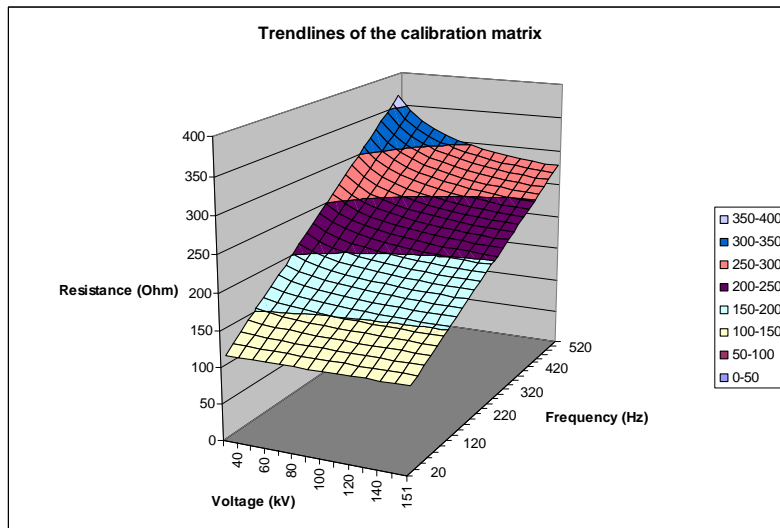


Figure 5-4: Trend lines show the relation between f , U and R

All lines are packed together and plotted in figure 5-4. Here, the 3D picture is given of this relation between frequency, voltage and internal resistance. This method appears to be promising, and is therefore further applied to a large number of calibration data.

5.2.2 Practical Support

In this section, several calibration matrices are analyzed as a function of frequency. With this information, a clear picture is given on the applicability of this method.

In the figures that follow, the following sub graphs are presented; in the upper left corner the current matrix (with capacitance axis) is plotted on a linear scale. In the upper right corner, the same graph is plotted on a linear scale, with one exception that the capacitance axis is transformed into a frequency axis. The graphs in the lower part are a 2D representation of the same images. Here, each line represents a voltage level. The Matlab code can be found in Appendix A.

5.2.2.1 A 28 kV DAC System

The first four graphs are from 28 kV DAC systems. Figure 5-5 shows the sensitivity of the transformation. In this matrix, all values for C are round off, and it can be seen that the linearity reduces with that action.

Figure 5-6 to 5-8 show three other 28 kV systems, but now with unrounded (and therefore more exact) values for the capacitance.

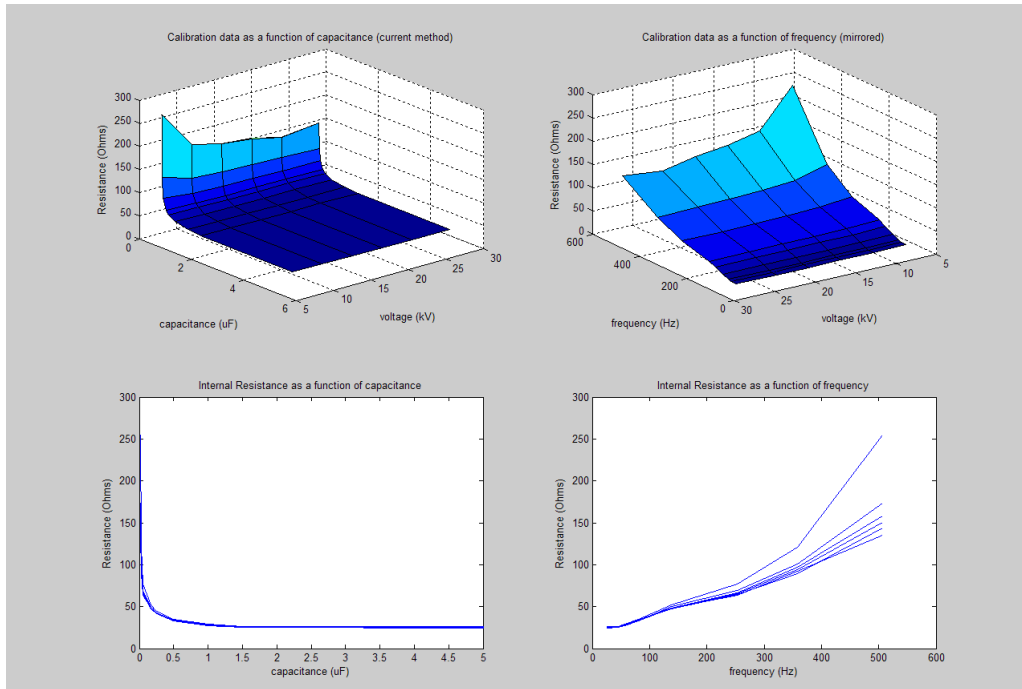


Figure 5-5: The calibration matrix of a 28 kV system (as a function of capacitance (round numbers) and frequency; 3D and 2D)

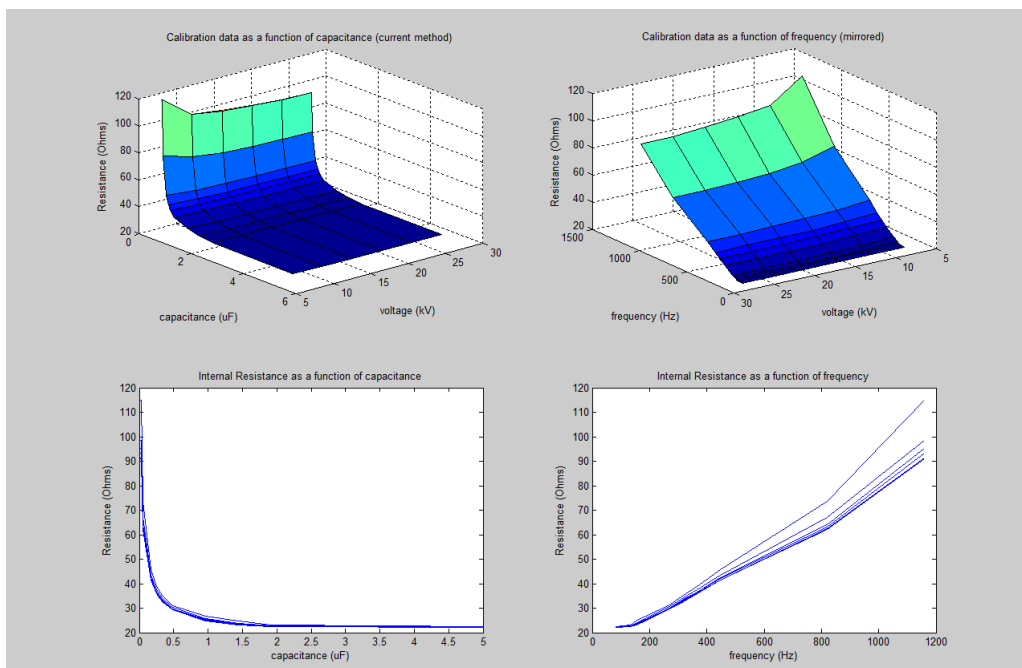


Figure 5-6: The calibration matrix of a 28 kV system (as a function of capacitance (unrounded numbers) and frequency; 3D and 2D)

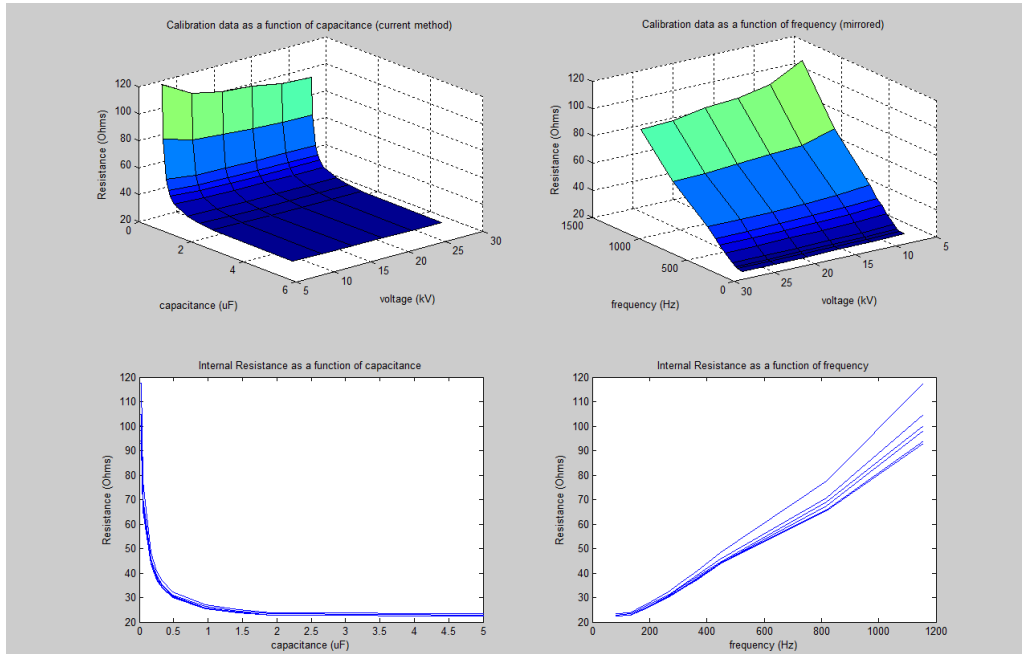


Figure 5-7: The calibration matrix of a 28 kV system (as a function of capacitance (unrounded values) and frequency; 3D and 2D)

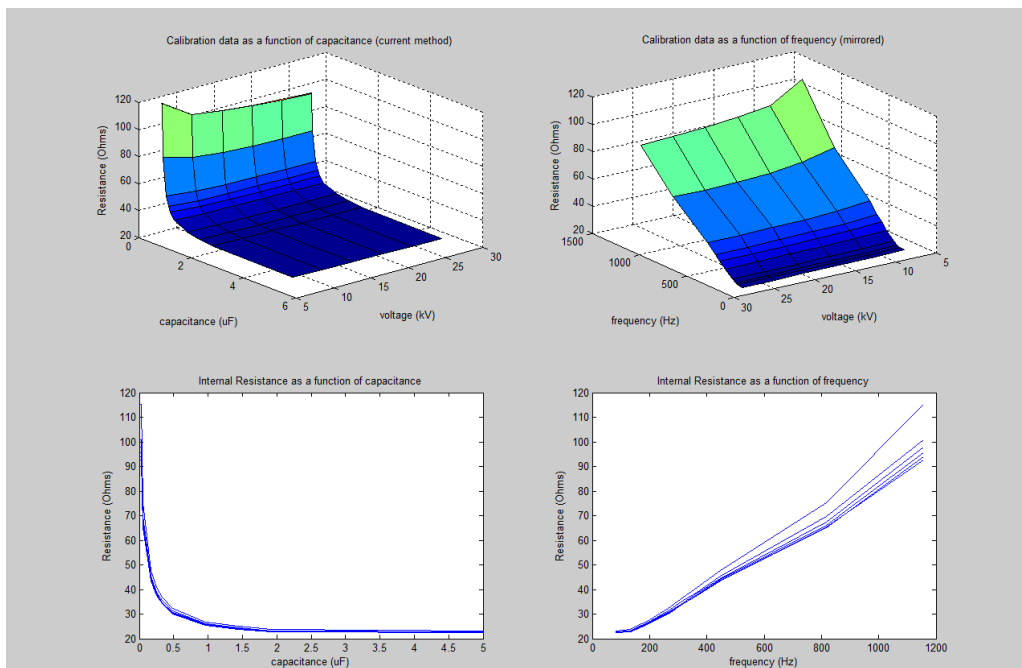


Figure 5-8: The calibration matrix of a 28 kV system (as a function of capacitance (unrounded values) and frequency; 3D and 2D)

5.2.2.2 A 60 kV DAC System

In this section, the same analysis is done on two 60 kV DAC systems. Figure 5-9 and 5-10 shows two 60 kV systems, both with unrounded values for the capacitance.

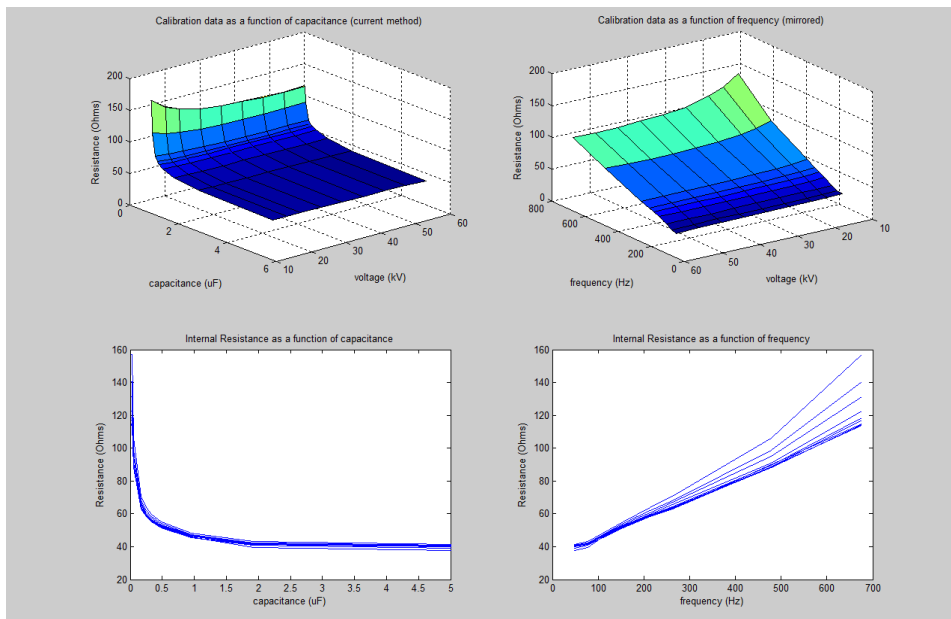


Figure 5-9: The calibration matrix of a 60 kV system (as a function of capacitance (unrounded values) and frequency; 3D and 2D)

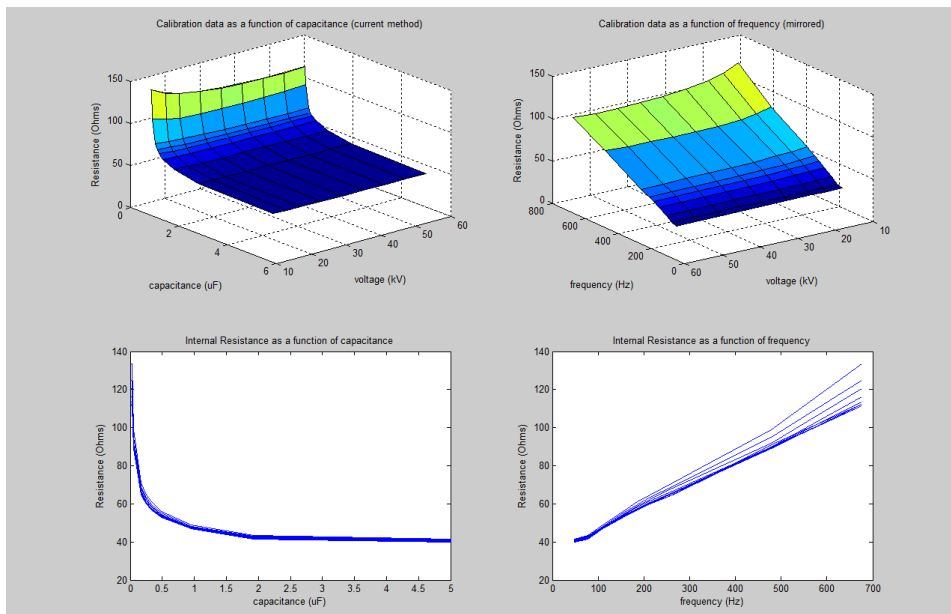


Figure 5-10: The calibration matrix of a 60 kV system (as a function of capacitance (unrounded values) and frequency; 3D and 2D)

5.2.2.3 A 150 kV DAC System

In this section, the same analysis is done on a 150 kV DAC system. Figure 5-11 shows the graphical counterpart of the calibration matrix of a 150 kV system.

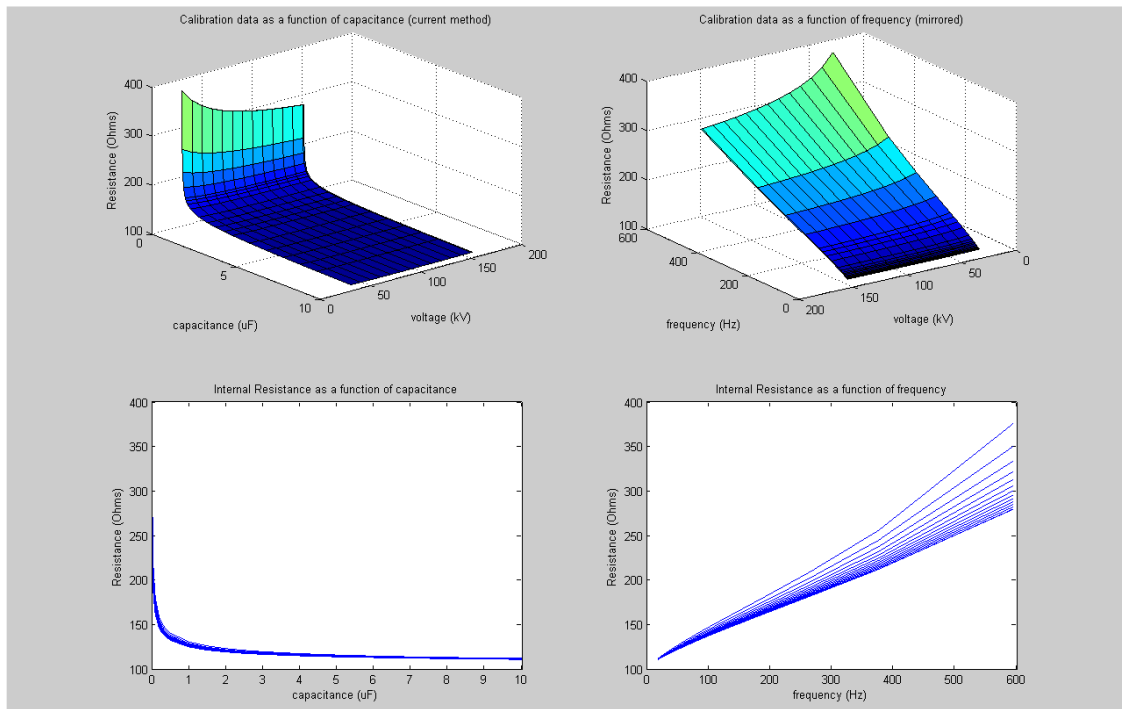


Figure 5-11: The calibration matrix of a 150 kV system (as a function of capacitance (unrounded values) and frequency; 3D and 2D)

5.2.3 Observations

From the analysis done on several DAC systems from different voltage classes, some observations can be made.

- The frequency representation of the internal resistance of the system gives an almost linear picture.
- When capacitance values are not sufficiently precise (e.g. by rounding off), this linearity gets distorted quite quickly.
- With declining voltage (within one system), the gradient of this linear approach becomes more steep.

In the following paragraph, a method is developed in which the frequency dependent graph is linearized with the use of two data points. This method is compared to the currently used one.

5.3 Linearization of the Frequency Representation

5.3.1 The Applied Method

At each voltage level, the frequency plot (shown in the previous section) will be linearized, and the effects on the accuracy of the dielectric loss calculation will be investigated. When this accuracy is sufficient, only 2 capacitance values are necessary for major part of the calibration, and the other values can be interpolated in the frequency domain.

The applied method is as follows; a straight line is drawn between the 2nd lowest and 2nd highest frequency (representing the 2nd highest and 2nd lowest capacitance). Since the lowest frequency (representing the highest capacitance) is a rounded value, and the highest frequency (representing the lowest capacitance) shows a deviation from the linear trend, these are therefore not incorporated.

The obtained values for the internal resistance are then used in the calculation of the loss tangent, and these values are then plotted as a function of voltage, for several frequencies.

In this way, it can be seen what the effects of a linear approach are on the loss tangent as a function of voltage.

The results of the linear approximations are given in figure 5-12. Here, the blue lines show the linear frequency plot of the calibration matrix in figure 5-6. The red lines show the linearization, where each line represents a separate voltage level.

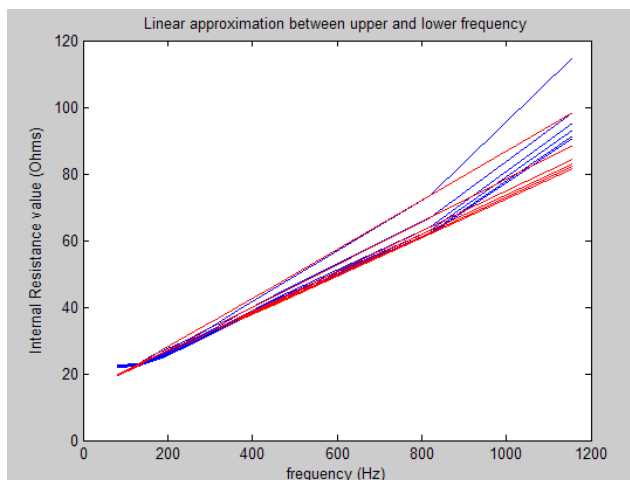


Figure 5-12: Linear approach between 2nd lowest and 2nd highest frequency of the system in figure 5-6

5.3.2 Validation of the Linear Method

In this section, the linear method is used to recalculate the dielectric losses from several systems. With this information, conclusions can be drawn on the accuracy and applicability of this new method.

Since the dielectric losses of the test capacitors and the internal resistance values are known, the obtained numbers for β can be fixed (according to formula [5-3], where only beta will then be unknown). When this value for beta will be kept fixed, and an internal resistance obtained from the linearization is entered into equation [5-3], the new DL (dielectric loss value) can be calculated. This is what will be done in the next figures.

With a constant value for the dielectric losses (DL=0.001), the results are given in figure 5-13. Here, the red line represents the current DL as a function of voltage, and the blue lines represent $\tan \delta$ as a function of voltage, for different frequencies (with a linearly approximated internal resistance (straight lines from figure 5-12)).

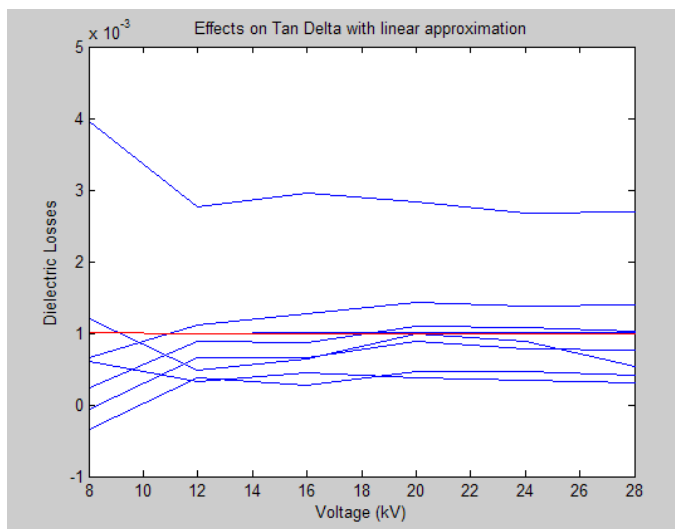


Figure 5-13: Tan delta obtained from the linear approximation of the internal resistance.

At the lowest voltage, a large deviation from the trend occurs. The upper blue line represents the highest frequency. As explained earlier, the blue lines are calculated with the red ($\tan \delta = 0.1\%$ line) as a reference.

In figure 5-14 and 5-15, the dielectric loss tangent is chosen to be represented as a rising curve. The calculation, as described earlier, is done again.

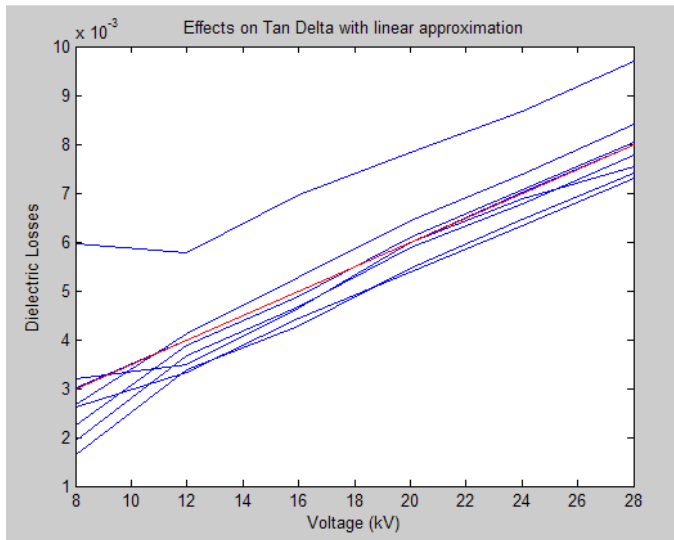


Figure 5-14: Tan delta obtained from the linear approximation of the internal resistance. Dielectric losses are rising from 0.3% at 8 kV up to 0.8% at 28 kV.

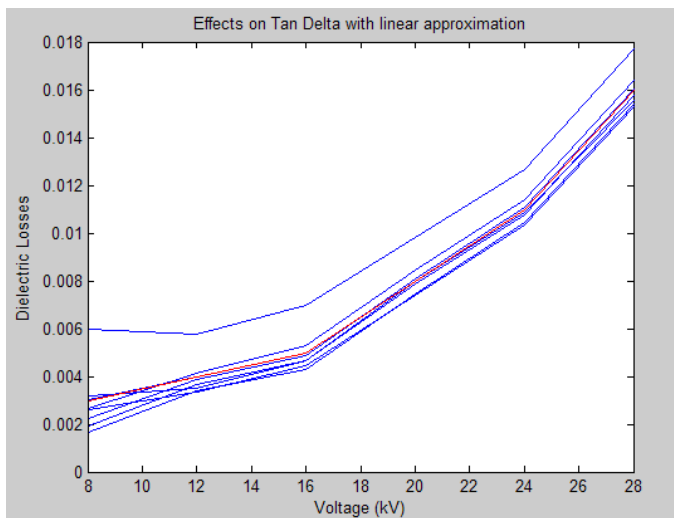


Figure 5-15: Tan delta obtained from the linear approximation of the internal resistance. Dielectric losses are exponentially rising from 0.3% at 8 kV up to 1.6% at 28 kV.

Again, one blue line shows a large deviation (the highest frequency that is left out of the linearization). It can be seen that the linear approximation method gives the same trend in dielectric losses as a function of voltage, compared to the current method (red line). The only visible difference is the reduced accuracy of the absolute value for the dielectric losses.

In the following 6 graphs, the same is done for a 60 kV DAC system and a 150 kV DAC system.

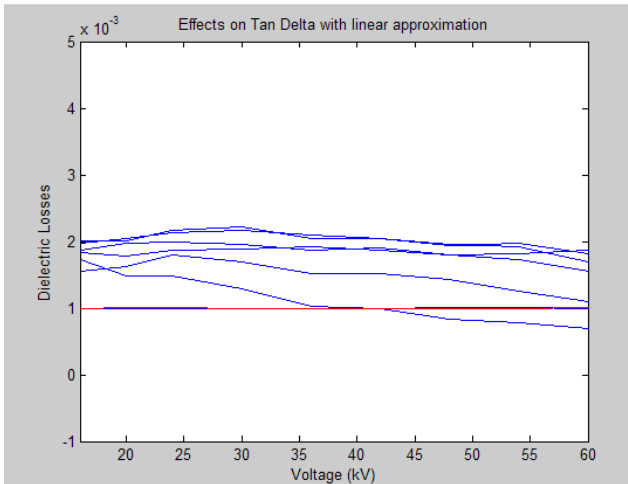


Figure 5-16: Tan delta obtained from the linear approximation of the internal resistance.

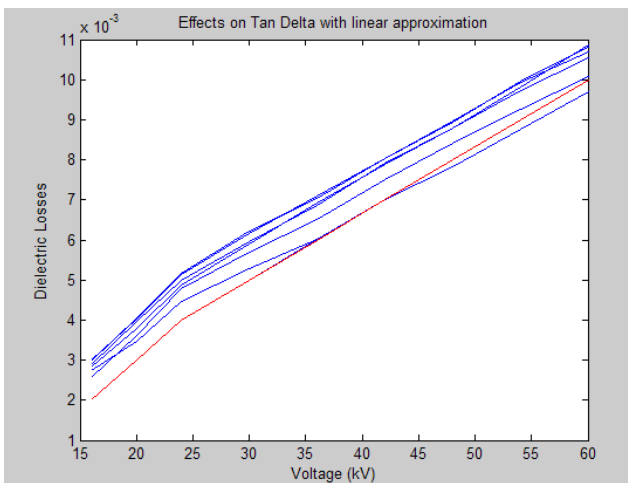


Figure 5-17: Tan delta obtained from the linear approximation of the internal resistance. Dielectric losses are rising from 0.2% at 15 kV up to 1.0% at 60 kV.

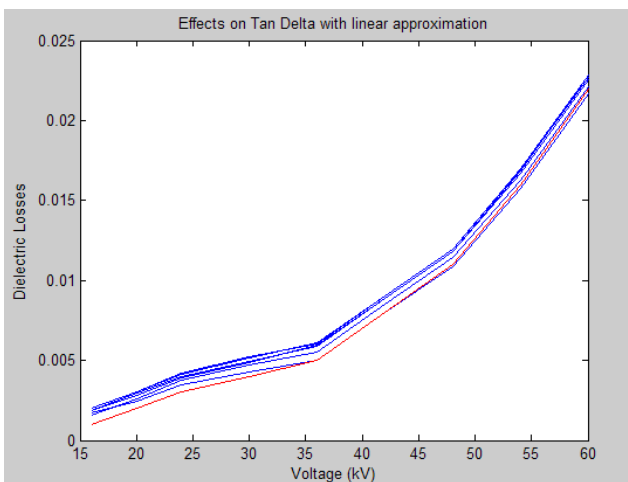


Figure 5-18: Tan delta obtained from the linear approximation of the internal resistance. Dielectric losses are exponentially rising from 0.1% at 15 kV up to 2.2% at 60 kV.

As shown in the previous calculations, the linear approach frequency suits well when the trendline is observed. In the next figures, a 150 kV system is analyzed.

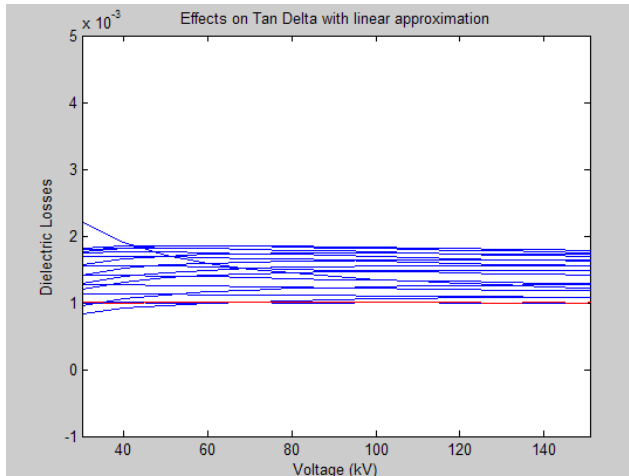


Figure 5-19: Tan delta obtained from the linear approximation of the internal resistance.

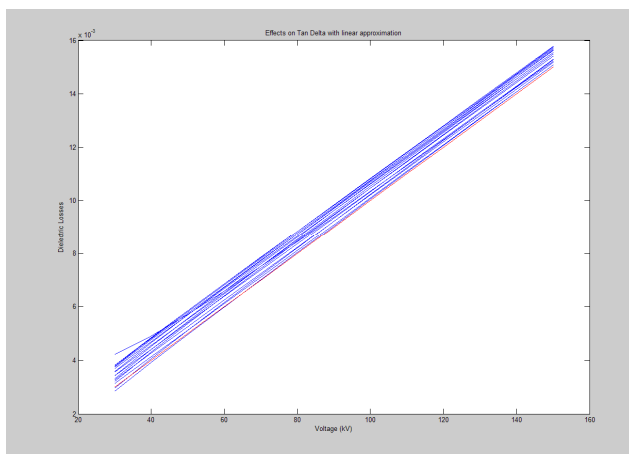


Figure 5-20: Tan delta obtained from the linear approximation of the internal resistance. Dielectric losses are rising from 0.3% at 30 kV up to 1.5% at 150 kV.

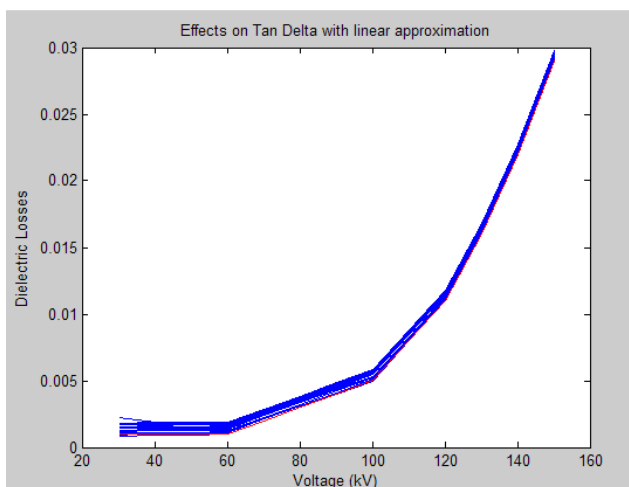


Figure 5-21: Tan delta obtained from the linear approximation of the internal resistance. Dielectric losses are exponentially rising from 0.1% at 30 kV up to 2.9% at 150 kV.

5.3.3 Remarks

Following the research on the linearized method of calibration, several remarks have to be made. These remarks are listed below.

- With the new linearization method, the voltage trend line of the dielectric losses remains the same, but the absolute value becomes more unstable in a wide range of frequencies.
- Due to this observation, it can only be concluded that although the frequency representation comes close to linearity, it is not enough to maintain the accuracy that it currently has. The more calibration points are introduced, the more accurate this method will be.
- Furthermore, in almost all cases, the earlier introduced approach is valid. When however physical changes are introduced, in order to reduce edge effects of the system at low voltages, this method cannot be applied. An example of such a system matrix (in capacitance representation) is shown in figure 5-22.

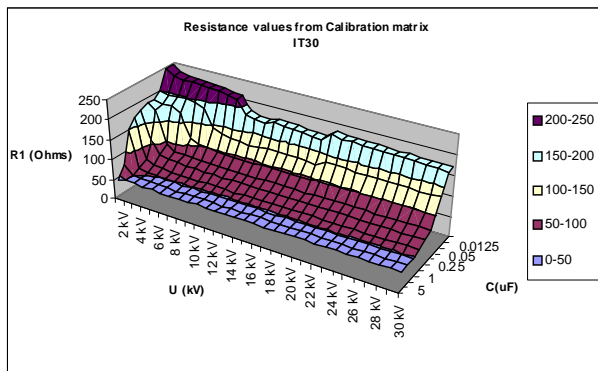


Figure 5-22:
DAC System with bypassed system components at lower voltages

Finally, the frequency representation is the major method that is introduced in this thesis. This choice is based on the fact that a simplification of the calibration process means, in general, less calibration points. Because this will lead to more interpolation, its accuracy is expected to be at its highest when this occurs in a linear related set of data. Since the frequency representation gives an (almost) linear picture, it is therefore investigated thoroughly.

5.4 Chapter Conclusions

Following the analysis done on calibration matrices from several systems (and consequently several voltage classes) some observations can be made and conclusions can be drawn.

- The use of a frequency scale results in a more linear depiction of the internal resistance values as a capacitance scale.
- When the voltage decreases, the slope of this linear frequency approach increases.
- Precise capacitance values (or frequency) are of importance to provide a more linear relationship. Capacitance values should not be rounded before constructing the table.
- In most systems, the lowest capacitance used (and thus the highest frequency modeled) shows a deviation from the linear trend. For that reason, a linearization has to take place between the obtained results from the 2nd highest and 2nd lowest capacitance, and therefore the 2nd lowest and 2nd highest frequency (at each voltage level).
- Linearization would reduce calibration time significantly, but should be avoided because of the decrease in absolute accuracy.

6. A COMPLETE OVERVIEW

6.1 Flow Chart

In this final chapter, an overview is presented on the steps that have to be taken in the determination of the dielectric losses from a damped AC voltage wave. A flowchart is shown first, in which a schematic insight is given into this procedure. In the next paragraph, an explanation on this flowchart is treated.

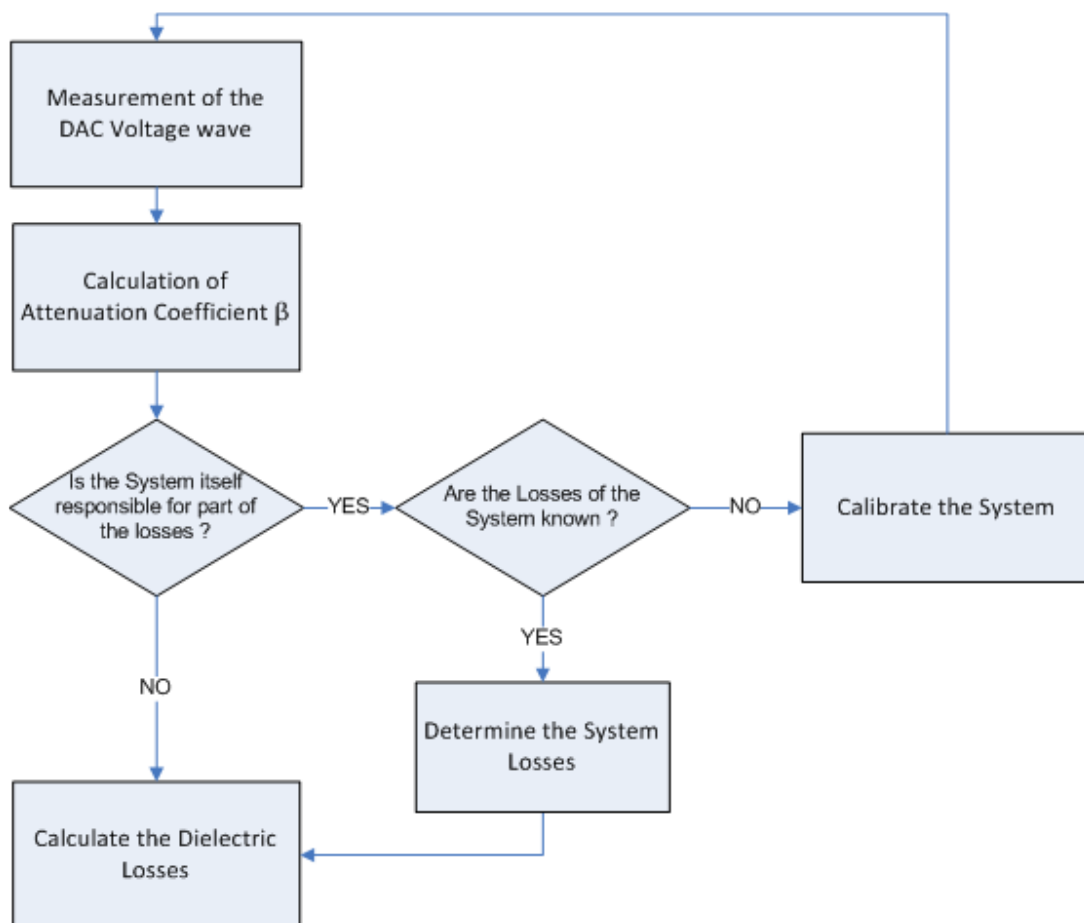


Figure 6-1: Flowchart of Dielectric Loss Estimation using Damped AC Voltages

6.2 Procedure Explanation

From the flowchart of figure 6-1, a detailed description is given here. Each process is treated separately.

Measurement of the DAC Voltage wave

The first action that has to be taken is the measurement of the DAC voltage wave. An introduction on the use of a DAC system is given below.

- *The system model*

A generally used model of a DAC system is shown in figure 6-2. It can be seen that, due to the principle of electrical resonance, the test object has to be mainly capacitive.

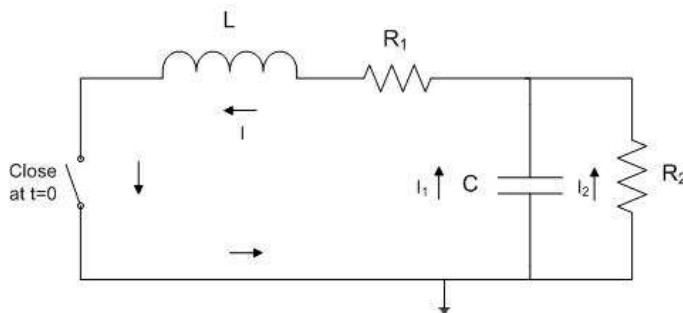


Figure 6-2: DAC-Model

In this model, L is the inductor, R1 is the total equivalent internal circuit resistance, C is the capacitance of the test object and R2 is the resistance of the test object, and therefore a measure for the dielectric losses. An important note is that this model is only valid for one frequency and voltage level at a time.

- *The measured DAC wave*

After charging the capacitive test object to the required test voltage, the switch will be closed and a so-called resonance occurs. Figure 6-3 shows the generated wave from a DAC system. Here, the attenuation is a measure for the dielectric losses in the test object.

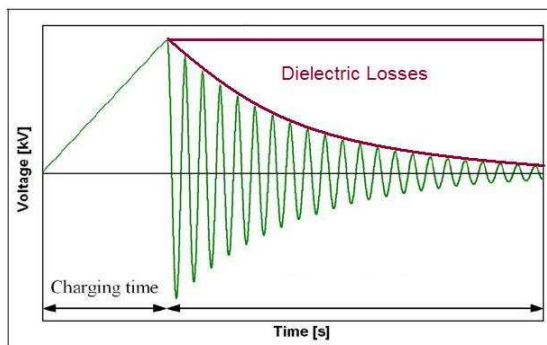


Figure 6-3: Charging and oscillation of a DAC voltage wave; the attenuation is a measure for the dielectric losses

This wave can be represented by equation [6-1], with β as the attenuation coefficient.

$$U(t) = e^{-\beta \cdot t} \sin(\omega \cdot t + \varphi) \quad [6-1]$$

Calculation of Attenuation Coefficient β

To calculate the losses from a measured DAC wave, the attenuation coefficient β has to be determined. This can be done by choosing two arbitrary peak values from the DAC wave (with corresponding time instants), and fill those into formula [6-2].

$$\frac{U_2}{U_1} = e^{-\beta(t_2 - t_1)} \Rightarrow \beta = -\frac{\ln\left(\frac{U_2}{U_1}\right)}{(t_2 - t_1)} \quad [6-2]$$

In order to calculate an attenuation that is most constant under different situations (voltage level, capacitance value, offset), a robust method would be to use the value for β that is calculated from the first two peaks, and averages it with β calculated from the first two lows (equation [6-3]).

$$\beta = \frac{\beta_{peak1-peak2} + \beta_{low1-low2}}{2} \quad [6-3]$$

The peak where the oscillation starts is not incorporated, so when the system is charged with negative polarity, low 1 will be the value after one full cycle.

Calibration of the System

In a theoretical DAC system, no internal losses will be present. In practice, this will of course be the case. To determine these losses, an extensive calibration procedure is required.

Due to the fact, that the internal resistance R1 is only valid for one voltage level and one frequency, it is necessary to determine this R1 value at different voltages and frequencies. The result will be a three dimensional relationship between U, f and R1.

To obtain these internal resistance values, several capacitors are used. These are then successively switched in series and parallel, to vary the total capacitance (and thus the frequency). Because the dielectric losses of these test capacitors are known, they can be extracted from total losses, and the system resistance values can be obtained

Equation [6-4] shows how to calculate this internal resistance from the measurement data. This equation is derived from the model in figure 6-2.

$$R_1 = 2\beta L - DL \cdot \omega L \quad [6-4]$$

Here, β is the measured attenuation coefficient, L is the inductance, DL is the known dielectric losses from the test capacitor and ω is the radial frequency.

Calculate the dielectric losses

The final step in the process of dielectric loss estimation is the calculation of this loss tangent. This is done with the use of equation [6-5].

$$DL = \frac{2\beta}{\omega} - \frac{R_1}{\omega L} \quad [6-5]$$

During a measurement in the field, the attenuation coefficient can be determined from the voltage wave. Together with the radial frequency and inductance, it can be filled into formula [6-5]. The test voltage and oscillation frequency are then used to obtain a corresponding value for R_1 .

Since the only unknown variable now becomes the dielectric losses DL , the final step in this process becomes an easy calculation.

7 ● CONCLUSIONS AND RECOMMENDATIONS

In this thesis, research has been performed on the dielectric loss estimation using damped AC voltages. From this investigation, several conclusions and recommendations follow.

Conclusions

The mathematical description of a DAC system is analyzed in twofold. One model contains a total equivalent internal resistance that represents all system losses; the other model contains a series (switch and coil) and parallel (voltage divider) resistance. It is investigated what the effects will be of a more detailed model for dielectric loss calculation.

It is concluded that;

1. The supplementary elements in the detailed mathematical model have (in theory) a negligible effect on the calculation of the dielectric losses.
2. To maintain the current accuracy, a detailed component calibration should be required. This is caused by the fact that each component is voltage and frequency dependent. As a result, the simplified model is therefore sufficient for use as a first approach.

The attenuation coefficient β , a measure for the damping of the voltage wave, has to be calculated with the use of two arbitrary voltage peaks, combined with the corresponding time instants. Using measurement data from the field, it is investigated what the most stable and robust method of calculation will be.

It is concluded that;

1. The attenuation coefficient, calculated by two arbitrary peaks or two arbitrary lows, can be considered relatively stable. A calculation that uses one peak and one low however becomes highly unstable.
2. In theory, it should not matter which two peaks/lows are used in the calculation; the attenuation coefficient should always be equal.
3. The analysis of the measurement data, combined with theoretical research, make it plausible that an voltage-offset is the main reason for an unstable calculation from one peak and one low.

4. To eliminate the effects of a possible offset, a new method has been proposed consisting of averaging β obtained from the first two peaks and first two lows. With the use of data from the field, it is proven to be a very robust method.

The internal system losses, as defined in the mathematical model, are voltage and frequency dependent. To determine the total internal equivalent resistance in a wide range of frequencies and voltages, a detailed calibration procedure is required. This results in a 3D relationship between voltage, capacitance and internal resistance.

It is concluded that;

1. The use of a frequency scale (instead of a capacitance scale) results in a more linear depiction of the internal resistance values.
2. A 3D relationship between voltage, frequency and internal resistance is suitable for linearization (and simplification of the procedure).
3. Although this method of linearization appears promising, the absolute value of the dielectric losses (in function of increasing voltage) becomes less accurate.
4. The current (detailed) calibration procedure has to be maintained.

Recommendations

The results in this thesis represent a fundamental improvement in the dielectric loss calculation using damped AC voltages. Nevertheless, topics are open for further research. Concerning this issue, the following recommendations are given;

1. Determine the influence of the sample frequency of the voltage wave on the accuracy of the attenuation coefficient calculation. It is presumed that, especially at higher frequencies, this sample frequency is of importance in the process that leads to the determination of the attenuation coefficient.
2. Do a practical research (measurements) on the main components in the system (coil, switches), and their behavior in function of voltage and frequency. With this information, a better insight in individual component behavior is obtained and a possible change or simplification of the current calibration procedure can be further examined.
3. The current calibration procedure is done manually. This means a time-consuming process. Some sort of automation of this process would not only lead to a reduction in time, but also eliminates the possibilities for human error.

REFERENCES

[1] F.H. Kreuger, *Industrial High Voltage*, volume 4,5,6., Delft University Press 1992.

[2] Website: http://en.wikipedia.org/wiki/Dielectric_spectroscopy

[3] Zaengl, W.S., "Dielectric spectroscopy in time and frequency domain for HV power equipment. I. Theoretical considerations," *Electrical Insulation Magazine, IEEE* , vol.19, no.5, pp.5-19, Sept.-Oct. 2003

[4] L. Chmura, Application of dielectric loss measurements for degradation assessment of oil-impregnated paper insulation in power cables, Master thesis. Delft University of Technology, 2009.

[5] E. Peschke, R. von Olshausen, *Cable Systems for High and Extra-High Voltage*, Publicis-MCD, 1999. ISBN 3-89578-118-5.

[6] Menzel, J.; Patsch, R.; Kamenka, D., "Measurement of the dielectric properties of paper-oil cables and the cellulose-oil insulation system of power transformers," *Properties and Applications of Dielectric Materials, 2009. ICPADM 2009. IEEE 9th International Conference on the* , vol., no., pp.1020-1025, 19-23 July 2009

[7] Patsch, R.; Kouzmine, O., "Return voltage measurements - the step from experimental data to a relevant diagnostic interpretation," *Electrical Insulating Materials, 2005. (ISEIM 2005). Proceedings of 2005 International Symposium on* , vol.3, no., pp. 889-892 Vol. 3, 5-9 June 2005

[8] Densley, J.; , "Ageing mechanisms and diagnostics for power cables - an overview," *Electrical Insulation Magazine, IEEE* , vol.17, no.1, pp.14-22, Jan.-Feb. 2001

[9] E. Gulski, Lecture slides, *Diagnostics for High Voltage Assets.*, Delft University of Technology, 2009.

[10] F.H. Kreuger, *Industrial High Voltage*, volume 1,2,3., Delft University Press 1992.

[11] Otowski, W.; Courteau, R.; Bose, T.K.; Lamarre, L., "Effect of temperature and time on the dissipation factor of power cable junctions," *Electrical Insulation and Dielectric Phenomena, 1993. Annual Report., Conference on* , vol., no., pp.763-768, 17-20 Oct 1993

- [12] Ildstad, E., "Dielectric response for condition assessment of PILC distribution cables," *Electrical Insulation and Dielectric Phenomena, 2003. Annual Report. Conference on* , vol., no., pp. 171-175, 19-22 Oct. 2003
- [13] Skjoelberg, J.; Hvidsten, S.; Farneo, H., "Experience from on-site condition assessment of XLPE MV cables," *Electrical Insulation, 2006. Conference Record of the 2006 IEEE International Symposium on* , vol., no., pp.432-435, 11-14 June 2006
- [14] H.J. van Breen, *Condition Assessment of Stator Insulation using Partial Discharge Diagnosis*, ISBN 90-9020128-9, Ph.D. thesis TU Delft, 2005.
- [15] Yanpeng Hao; Zhidong Jia; Xiongwei Jiang; Naikui Gao; Hengkun Xie; , "The changes of mechanical properties of epoxy/mica insulation materials in aging process," *Properties and Applications of Dielectric Materials, 2000. Proceedings of the 6th International Conference on* , vol.1, no., pp.185-188 vol.1, 2000
- [16] IEC Standard, Rotating electrical machines - Part 27 : Off-line partial discharge measurements on the stator winding insulation of rotating electrical machines (IEC/TS 60034-27:2006,IDT)
- [17] Hudon, C.; Bartnikas, R.; Wertheimer, M.R.; , "Effect of physico-chemical degradation of epoxy resin on partial discharge behavior," *Dielectrics and Electrical Insulation, IEEE Transactions on* , vol.2, no.6, pp.1083-1094, Dec 1995
- [18] Oyegoke, B.; Hyvonen, P.; Aro, M.; Gao, N., "Selectivity of damped AC (DAC) and VLF voltages in after-laying tests of extruded MV cable systems," *Dielectrics and Electrical Insulation, IEEE Transactions on* , vol.10, no.5, pp. 874-882, Oct. 2003
- [19] Uchida, K.; Kobayashi, S.; Kawashima, T.; Tanaka, H.; Sakuma, S.; Hirotsu, K.; Inoue, H., "Study on detection for the defects of XLPE cable lines," *Power Delivery, IEEE Transactions on* , vol.11, no.2, pp.663-668, Apr 1996
- [20] Salter, E. H, "Guarding and Shielding for Dielectric Loss Measurement on Short Lengths of High-Tension Power Cable," *American Institute of Electrical Engineers, Transactions of the* , vol.48, no.4, pp.1294-1299, Oct. 1929
- [21] Patsch, R.; Jochen Jung; Kouzmine, O., "The interpretation of return voltage curves of paper-oil-cables," *Electrical Insulation and Dielectric Phenomena, 2000 Annual Report Conference on* , vol.1, no., pp.39-42 vol.1, 2000

[22] Kozlovskis, A.; Rozenkrons, J., "Temperature dependence of return voltage characteristics," *Power Delivery, IEEE Transactions on*, vol.14, no.3, pp.705-708, Jul 1999

[23] F.J. Wester, *Condition Assessment of Power Cables Using PD Diagnosis at Damped AC Voltages*, ISBN 90-8559-019-1, Ph.D. thesis TU Delft, 2004.

[24] Nilsson / Riedel, *Electric Circuits*. Pearson Education Inc., 2008, ISBN 0-13-198925-1, pag. 308-310.

[25] C.K. Alexander / M.N.O. Sadiku, *Fundamentals of Electrical Circuits*. McGraw Hill, Third Edition 2007, ISBN-10-0-07-297718-3, pag. 326-327.

[26] *Basic Electronics*, Dover Publications Inc., 1973, ISBN-0-486-21076-6, pag. 194-202.

[27] A. Stenger / B. Girod / R. Raberstein, *Signals and Systems*. John Wiley and Sons, 2001, ISBN-978-0471988007.

APPENDIX A:

MATLAB CODE MSc THESIS

1. Create Artificial DAC Wave

```
function y = dampedcosine(b,X)

a=b(1);
beta=b(2);
omega=b(3);
theta=b(4);

y = a .* exp(-beta*X) .* cos(omega*X+theta);
```

2. DAC Curve Fitting

```
x=[0:1.25e-5:10e-2];
b=[-30 18 1 3.14];
y=dampedcosine(b,x);
time=x';
q=nlinfit(time(start:stop),data(start:stop),@dampedcosine,b)
y=dampedcosine(q,time');
plot(y)
axis([0 length(data) -130 130])
hold on
plot(data,'red')
'the measured data is red'
```

3. Visualize and Linearize Calibration Data

```
C=(Matrix(1,2:size(Matrix,2)));
U=(Matrix(2:size(Matrix,1)-1,1));
L=2.22;
f=[];

subplot(2,2,1)
[x,y]=meshgrid(C,U);
surf(x,y,Matrix(2:size(Matrix,1)-1,2:size(Matrix,2)))
view(50,30)

title('Calibration data as a function of capacitance (current method)')
xlabel('capacitance (uF)')
ylabel('voltage (kV)')
zlabel('Resistance (Ohms)')

for x=1:1:length(C),
f(x)=1/(2*pi()*sqrt(L*C(x)*1e-6));
end
```

```

subplot(2,2,2)
[x,y]=meshgrid(f,U);
surf(x,y,Matrix(2:size(Matrix,1)-1,2:size(Matrix,2)))
view(235,30)

title('Calibration data as a function of frequency (mirrored)')
xlabel('frequency (Hz)')
ylabel('voltage (kV)')
zlabel('Resistance (Ohms)')

subplot(2,2,3)
for x=2:1:size(Matrix,1),
plot(C,Matrix(x,2:size(Matrix,2)))
hold on
title('Internal Resistance as a function of capacitance')
xlabel('capacitance (uF)')
ylabel('Resistance (Ohms)')
end

subplot(2,2,4)
for x=2:1:size(Matrix,1),
plot(f,Matrix(x,2:size(Matrix,2)))
hold on
title('Internal Resistance as a function of frequency')
xlabel('frequency (Hz)')
ylabel('Resistance (Ohms)')
end

figure
f=f(1:length(f)-1);
Linear=[];

% richtingscoefficienten in matrix stoppen
for x=2:1:size(Matrix,1)-1,
Linear(x-1,1)=((Matrix(x,size(Matrix,2)-1)-Matrix(x,3))/(f(length(f))-f(2)));
Linear(x-1,2)=(Matrix(x,3)-Linear(x-1,1)*f(2));
end

Reslin=[];
Rlinmat=[];

for v=1:1:size(Linear,1),
for x=1:1:length(f),
Reslin(x,1)=f(x);
Reslin(x,2)=Linear(v,1)*f(x)+Linear(v,2);
Reslin(x,3)=Matrix(v+1,x+1);

end
plot(f,Matrix(v+1,2:size(Matrix,2)-1))

```

```

    hold on
    plot(Reslin(:,1),Reslin(:,2),'red')

end

for y=1:1:size(Matrix,1)-2,
for x=1:1:size(Matrix,2)-2,
    Rlinmat(y,x)=(Linear(y,1)*f(x)+Linear(y,2));
end
end

DL=[];
DL=zeros(size(Rlinmat,1),size(Rlinmat,2));
TAN=0.001;

for x=1:1:size(DL,1),
    DL(x,:)=DL(x,:)+TAN;
    TAN=TAN-0.000;
end

beta=[];
tand=[];
tandlin=[];

for y=1:1:size(Matrix,1)-2,
for x=1:1:size(Matrix,2)-2,
    beta(y,x)=(0.5*DL(y,x)*2*pi()*f(x))+((Matrix(y+1,x+1))/(2*L));
end
end

for y=1:1:size(Matrix,1)-2,
for x=1:1:size(Matrix,2)-2,
    tand(y,x)=(2*beta(y,x)/(2*pi()*f(x)))-((Matrix(y+1,x+1))/(2*pi()*f(x)*L));
end
end

for y=1:1:size(Matrix,1)-2,
for x=1:1:size(Matrix,2)-2,
    tandlin(y,x)=(2*beta(y,x)/(2*pi()*f(x)))-((Rlinmat(y,x))/(2*pi()*f(x)*L));
end
end

figure
for t=2:1:size(tandlin,2),
    plot(U(1:length(U)), tandlin(1:size(Matrix,1)-2,t))
    hold on
end

plot(U, tandlin(:,2),'red')

```


APPENDIX B:

CMD 2010 CONFERENCE PROCEEDING

Estimation of Dielectric Loss using Damped AC Voltages

Richard Houtepen^{1*}, Edward Gulski¹, Johan J Smit¹ and Ben Quak²

¹ High Voltage Technology and Management, Delft University of Technology, Delft, The Netherlands

² Seitz Instruments AG, Niederrohrdorf, Switzerland

*E-mail: s.a.a.houtepen@student.tudelft.nl

Abstract—Insulation failures in HV components may be caused by lower dielectric strength due to aging processes and by internal defects in the insulation system. It is known, that unlike voltage testing, measurements of the dielectric loss may give an absolute indicator for the quality level of the cable insulation. Since several years the application of damped ac voltages for testing and diagnosis of HV components like power cables and stator insulation is well known.

This contribution is focused on the application of dielectric loss measurements to the insulation of service components. In particular, to discuss the principles of dielectric loss estimation using damped AC voltages theoretical investigation, calculation procedures will be presented and verified on laboratory experiments and field measurements.

Keywords: Dielectric Losses; Damped AC; On-Site Diagnosis; Condition Assessment

I. INTRODUCTION

Nowadays, many advanced methods for condition assessment of service-aged HV components are available [1]. These condition assessment diagnostics, which are applied to service-aged HV systems, are not only based on a pass or fail criterion. During such a test, attention is paid to recognize, localize and evaluate possible defects. When this is done periodically, evaluation of these processes in time can be monitored. The main purposes of condition assessment of HV equipment are listed hereunder [2]:

- To check the availability and reliability of the component
- By non-destructive diagnostics, it can be estimated what the actual condition of the service-aged system is, and a check is performed on the insulation degradation after a period in time.
- Reference values of the diagnostic tools are provided and can be used for later tests (in order to demonstrate whether the insulation is still free from dangerous defects and that the life-time expectation is sufficiently high)
- Diagnostic measurements can demonstrate that a component has been successfully repaired after a failure and the defect in the insulation is eliminated

To assess the dielectric properties of high-voltage equipment in service, non-destructive methods are used. Dielectric loss measurement is one of most important diagnostic tools for condition assessment of e.g. oil-filled cables.

Since 10 years, the use of damped AC (DAC) voltages is a well known method to determine $\tan \delta$. In particular the estimation of dielectric loss parameter is based on the estimation of the DAC voltage attenuation, and numeric procedures are used. To achieve sufficient sensitivity (at this moment 0.1%), each type of system has to be subjected to a detailed calibration procedure. Due to the fact, that damped AC voltage becomes more and more a standard solution for on-site diagnosis of all types of oil-filled power cables up to 380kV and stator insulation of electrical machines [3] [4], systematic research is done to optimize the procedure of dielectric loss estimation.

II. DAMPED AC VOLTAGES

A. Principle

The damped AC method makes use of a linear charging current, after which the capacitive test component oscillates with an air core inductor. Therefore no reactive power is necessary. This is an important factor, because it drastically reduces the size of the test equipment.

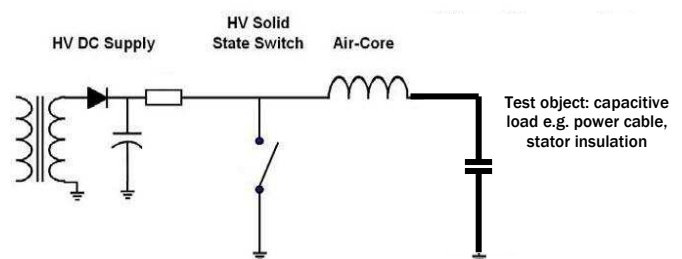


Figure 1. Schematic View of a DAC System

A schematic overview of a DAC system is given in figure 1. For the generation of DAC voltages, a capacitive load (the test object) is first charged with a DC power supply. After charging, the capacitive load is directly switched in series with an external inductor [5] [6]. The resulting graph of this process is given in figure 2.

The originated voltage wave can be simply described by (1) [7]. Here, the attenuation coefficient β is responsible for the decay of the wave and therefore a measure for the dielectric losses in the test object.

$$U(t) = U_0 \cdot e^{-\beta \cdot t} \sin(\omega \cdot t + \varphi) \quad (1)$$

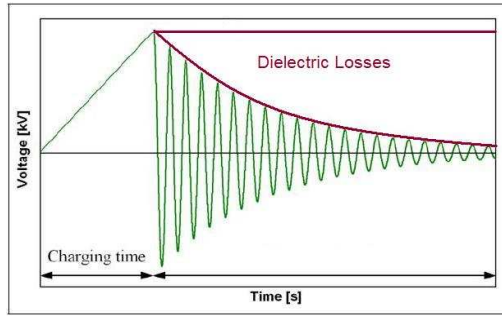


Figure 2. The Attenuation of the DAC voltage is a measure for the Dielectric Losses in the test object

B. Loss Calculation

A damped AC system uses the principle of electrical resonance, to measure partial discharges and determine dielectric losses. Its topology is in principle a series RLC circuit. Figure 3 shows a circuit model for a DAC system. This model is only valid for one frequency and/or voltage at a time.

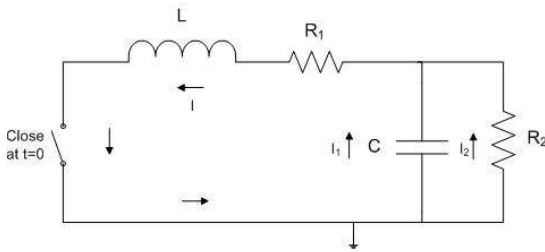


Figure 3. Circuit Model for a DAC System

In this model, R1 represents the total internal resistance of the system, whereas R2 represents the losses in the test object, which are thus a measure for the loss tangent. From this model, a mathematical relation can be derived that exists between the attenuation coefficient and the loss tangent. (2) gives an expression for resistance R2.

$$R_2 = \frac{L}{2\beta LC - R_1 C} \quad (2)$$

From this equation, R2 can be used in the generally known equation for the calculation of $\tan \delta$, as can be seen in (3).

$$\tan(\delta) = \frac{1}{\omega R_2 C} \quad (3)$$

From (2), it is shown that the attenuation coefficient β , inductance L, capacitance of the test object C and internal resistance R1 have to be determined in order to calculate the dielectric losses.

$$f_0 = \frac{1}{2\pi\sqrt{LC}} \quad (4)$$

Since the inductance of the system is known, and the capacitance can be calculated with the use of the oscillation frequency (4), only the attenuation coefficient β and internal resistance R1 have to be determined. The exact relation between the dielectric losses (DL) and these two unknown parameters is given in (5).

$$DL = \frac{2\beta}{\omega} - \frac{R_1}{\omega L} \quad (5)$$

III. THE ATTENUATION COEFFICIENT

A. Measurement Data Analysis

In the given mathematical presentation, the attenuation coefficient β is a measure for the losses in the system and test object. The loss calculation is therefore based on this one key variable.

$$\frac{U_2}{U_1} = e^{-\beta(t_2 - t_1)} \Rightarrow \beta = -\frac{\ln\left(\frac{U_2}{U_1}\right)}{(t_2 - t_1)} \quad (6)$$

In general, two peaks (positive and/or negative) are taken from the measured voltage wave. Combined with the corresponding time instants, it will lead to a value for the attenuation coefficient. Eq. (6) shows the calculation method of β from the measured voltage wave.

In theory, two arbitrary peaks and/or lows can be used to solve eq. (6) and despite the choice, it consequently leads to the same outcome for the attenuation coefficient. In practice however, the outcome differs. In the following figure, the calculation is shown in function of one peak and one low combined (figure 4). The first peak/low that is used in the calculation is given in the index of each figure, the second peak/low can be found on the x-axis. The results show that especially the calculation from one peak and one low gives a very unstable behavior.

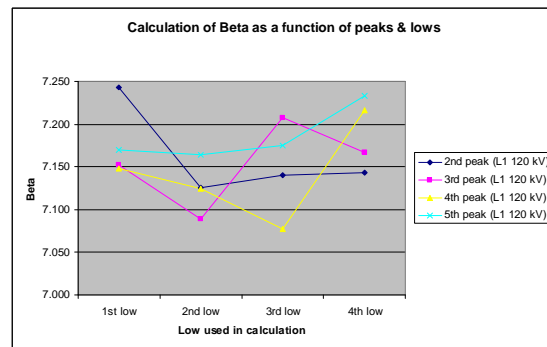


Figure 4. Attenuation as a function of peaks and lows of a 120 kV oil impregnated cable in a 120 kV test. The total cable length is 5300 meters

B. A New Calculation Method for β

From the data analysis on measurements from the field, it is plausible that an offset is the main reason for the behavior of the attenuation coefficient in function of peaks and lows combined.

In order to calculate an attenuation that is most constant under different situations (voltage level, capacitance value, offset), a robust method would be to use the value for β that is calculated from the first two peaks, and averages it with β calculated from the first two lows (according to (7)).

$$\beta = \frac{\beta_{\text{peak1-peak2}} + \beta_{\text{low1-low2}}}{2} \quad (7)$$

The peak where the oscillation starts is not incorporated, so when the system is charged with e.g. negative polarity, the first low will be the value after one full cycle of the DAC wave. In figure 7, a comparison is made between calculation from two peaks, from two lows and with the use of the new method (as introduced in eq. (7)).

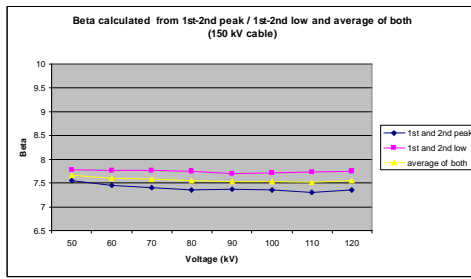


Figure 5. Attenuation as a function of increasing voltage as a function of peak-peak, low-low and newly introduced averaging method.

When the voltage dependency of the damping is examined, the same trendline is visible when comparing the current method and the newly introduced one. This is of great importance, since $\Delta \tan \delta$ is a valuable parameter to determine the condition of the test object. Furthermore, errors that are caused by a possible offset can be (partially) corrected as can be seen in figure 5.

IV. THE INTERNAL SYSTEM LOSSES

A. System Calibration

As was earlier presented in figure 3, the system itself is responsible for part of the losses. This total equivalent internal resistance R_1 represents the losses for one voltage level and/or frequency at the time. Therefore, an extensive calibration procedure is necessary to determine this R_1 value at different voltages and frequencies. The result will be a three dimensional relationship between U , C and R_1 . Figure 6 shows a graphical representation of such a table.

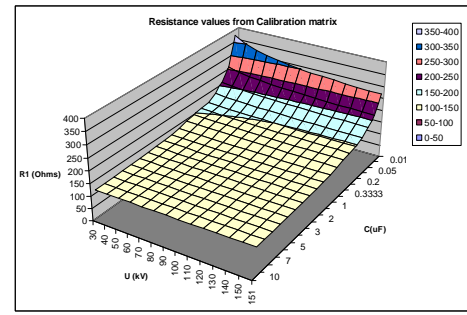


Figure 6. 3-Dimensional relationship between U , C and R_1

To obtain the internal resistance values, several capacitors are used. These are then successively switched in series and parallel, to vary the total capacitance (and thus the frequency) in a complete range of system voltages. Since the dielectric losses of the test capacitors are known, the internal resistances can then be calculated, as described in equations (2) and (3).

During a measurement in the field, the test voltage and oscillation frequency are used to obtain a corresponding value for R_1 from the data. All together, it goes without saying that this whole calibration procedure is very time-consuming and elaborate, but at the same time very accurate.

B. Linearization of the Data

Due to the asymptotical behavior of the internal resistance values at lower capacitances, it is chosen to translate the capacitance axis into a frequency axis (eq. 4). Since a simplified calibration means, in general, less calibration points, an experimental approach is chosen where the relation between internal resistance and frequency becomes linear.

When this operation is performed at several voltage levels, the 3D relation between U , f and R_1 (same as in figure 6) originates. This is shown in figure 7.

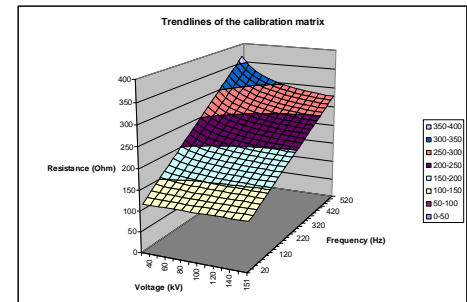


Figure 7. 3-Dimensional relationship between U , f and R_1

In this example, it is obvious that such an approach of the internal resistance values is suitable for a linearization. This linearization would simplify the calibration of a DAC system.

After investigation, it can be said that although the voltage trend lines are comparable with increasing voltage, the absolute value is less stable then in the current method. Linearization would reduce calibration time significantly, but should be avoided because of the decrease in absolute accuracy.

V. OVERVIEW AND DISCUSSION

A. Flowchart DL Measurement using DAC

The flowchart in figure 8 shows a complete overview on the dielectric loss measurement procedure with DAC voltages.

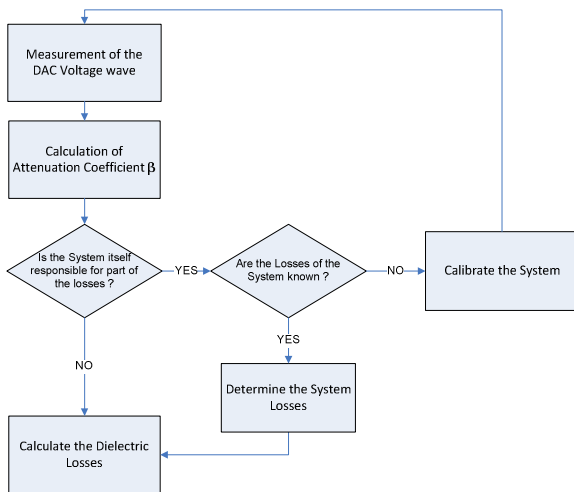


Figure 8. Flowchart of complete Dielectric Loss Measurement procedure using DAC voltages.

B. AC versus DAC

In practical applications, the dielectric losses are often measured around 0.1 Hz (VLF), 50 Hz (grid frequency) or several hundreds of Hz (DAC). Since it is known that these losses are frequency dependent, it is of interest whether it makes sense to measure losses at a different frequency than the one normally applied in the grid.

In practice, when a healthy dielectric is taken, the conductivity is very low. It is furthermore noticeable, that the dielectric constant (real and imaginary part) is however slowly declining in theory, but will be more or less stable (up to 1 kHz) in reality. It can be seen in figure 9, that dielectric loss measurement using damped AC voltages is a very useful tool that gives reliable results when compared to a measurement performed at 50 Hz.

Example 1			Example 2		
C=0.137uF	Tan delta measurement [%]		C=0.049uF	Tan delta measurement [%]	
Voltage	292Hz DAC	50Hz AC	Voltage	490Hz DAC	50Hz AC
0.4Un	3.10	3.0	0.4Un	3.7	3.3
0.6Un	3.11	3.0	0.6Un	3.73	3.3
0.8Un	3.11	3.1	0.8Un	3.82	3.4
1.0Un	3.12	3.2	1.0Un	3.89	4.2

Figure 9. Two measurements, both performed with DAC and AC, show the effectiveness of dielectric loss measurement using damped AC.

It is thus definitely sensible to measure at a frequency that differs from the one used in the power grid, in order to obtain a clear picture on the condition of the dielectric.

VI. CONCLUSIONS AND DISCUSSION

Research is done on the dielectric loss estimation using damped AC voltages. From this investigation, several conclusions follow:

- The supplementary elements in the detailed mathematical model have (in theory) a negligible effect on the calculation of the dielectric losses. As a result, the simplified model is sufficient for use as a first approach.
- The attenuation coefficient, calculated by two arbitrary peaks or two arbitrary lows, can be considered relatively stable. A calculation that uses one peak and one low becomes highly unstable.
- The analysis of the measurement data, combined with theoretical research, make it plausible that an offset is the main reason for an unstable calculation from one peak and one low.
- To eliminate the effects of a possible offset, a new method has been proposed consisting of averaging β obtained from the first two peaks and first two lows. With the use of data from the field, it is proven to be a very robust method.
- The use of a frequency scale (instead of a capacitance scale) results in a more linear depiction of the internal resistance values. A 3D relationship between voltage, frequency and internal resistance is suitable for linearization (and simplification of the procedure).
- Although this method of linearization appears promising, the absolute value of the dielectric losses (in function of increasing voltage) becomes less accurate. The current (detailed) calibration procedure has to be maintained.

REFERENCES

- [1] Z.Á. Tamus, E. Németh, *Measurement of Dielectric, Mechanical and Chemical Properties of the Insulation in Cable Diagnostic*, Proceedings 15th Int. Symp. HV Eng., ISH 2007, Ljubljana, Slovenia, T8-739.
- [2] E. Gulski, J.J. Smit, F.J. Wester, *PD knowledge rules for insulation condition assessment of distribution power cables*. IEEE Transactions on dielectrics and electrical insulation, 2005
- [3] Gulski, E., Quak, B., Seitz, P.P., Vries, F. de (2008). *Partial discharge diagnosis of stator insulation using damped AC voltages*. In T. House (Ed.), *Inductica 2008 Conference proceedings Vol. 32. Coil winding international & electrical insulation magazine* (pp. 1-8). Alderney, Channel Islands: Coil Winding International Ltd.
- [4] H.J. van Breen, *Condition Assessment of Stator Insulation using Partial Discharge Diagnosis*, ISBN 90-9020128-9, Ph.D. thesis TU Delft, 2005.
- [5] P.P. Seitz, B. Quak, E. Gulski, J.J. Smit, P. Cichecki, F. de Vries, F. Petzold, *Novel Method for On-site Testing and Diagnosis of Transmission Cables up to 250kV*, Proceedings Jicable '07. 7th Intern. Conf. Insulated Power Cables, Versailles, France, Paper 16, 2007.
- [6] F.J. Wester, *Condition Assessment of Power Cables Using PD Diagnosis at Damped AC Voltages*, ISBN 90-8559-019-1, Ph.D. thesis TU Delft, 2004.
- [7] A. Stenger / B. Girod / R. Raberstein, *Signals and Systems*. John Wiley and Sons, 2001, ISBN-978-0471988007.